Front. Phys. China, 2007, 2(3): 327－357
DOI 10.1007/s11467-007-0037-0

REVIEW ARTICLE

CHEN Lie-wen, KO Che Ming, LI Bao-an, YONG Gao-chan

Probing the nuclear symmetry energy with heavy-ion reactions induced by neutron-rich nuclei

© Higher Education Press and Springer-Verlag 2007

Abstract Heavy-ion reactions induced by neutron-rich nuclei provide a unique means to investigate the equation of state of isospin-asymmetric nuclear matter, especially the density dependence of the nuclear symmetry energy. In particular, recent analyses of the isospin diffusion data in heavy-ion reactions have already put a stringent constraint on the nuclear symmetry energy around the nuclear matter saturation density. We review this exciting result and discuss its implications on nuclear effective interactions and the neutron skin thickness of heavy nuclei. In addition, we also review the theoretical progress on probing the high density behaviors of the nuclear symmetry energy in heavy-ion reactions induced by high energy radioactive beams.

Keywords nuclear equation of state, symmetry energy, neutron-rich matter, heavy-ion reactions, radioactive beams, transport theory

PACS numbers 25.70.-z, 21.30.Fe, 24.10.Lx

CHEN Lie-wen
Institute of Theoretical Physics, Shanghai Jiao Tong University, Shanghai 200240, China
Center of Theoretical Nuclear Physics, National Laboratory of Heavy Ion Accelerator, Lanzhou 730000, China

KO Che Ming
Cyclotron Institute and Physics Department, Texas A&M University, College Station, Texas 77843-3366, USA

CHEN Lie-wen, LI Bao-an (✉), YONG Gao-chan
Department of Physics, Texas A&M University-Commerce, Commerce, Texas 75429-3011, USA
E-mail: Bao-An_Li@tamu-commerce.edu

YONG Gao-chan
Institute of Modern Physics, Chinese Academy of Sciences, Lanzhou 730000, China
Graduate School, Chinese Academy of Sciences, Beijing 100039, China

Received April 17, 2007

1 Introduction

During the last decade, many radioactive beam facilities have become available in the world. At these facilities, nuclear reactions involving nuclei with large neutron or proton excess can be studied, providing the opportunities to study the properties of nuclear matter under the extreme condition of large isospin asymmetry. This has led to a lot of interest and activities in a new research direction in nuclear physics, namely the isospin physics. The ultimate goal of studying isospin physics is to extract information on the isospin dependence of in-medium nuclear effective interactions as well as the equation-of-state (EOS) of isospin asymmetric nuclear matter, particularly its isospin-dependent term, i.e., the density dependence of the nuclear symmetry energy. There are already extensive reviews on isospin physics in nuclear physics, and they can be found in, e.g., Refs. [1–6].

Knowledge about the nuclear symmetry energy extracted from the EOS of isospin asymmetric nuclear matter is essential in understanding not only many aspects of nuclear physics, such as heavy-ion collisions induced by radioactive nuclei and the structure of exotic nuclei, but also a number of important issues in astrophysics, such as nucleosynthesis during pre-supernova evolution of massive stars and the cooling of protoneutron stars. Although the nuclear symmetry energy at normal nuclear matter density is known to be around 30 MeV from the empirical liquid-drop mass formula [7, 8], its values at other densities, especially at supra-normal densities, are poorly known [1, 2]. Predictions based on various many-

body theories differ widely at both low and high densities [9, 10]. Empirically, the incompressibility of asymmetric nuclear matter is essentially undetermined [11], even though the incompressibility of symmetric nuclear matter at its saturation density $\rho_0 \approx 0.16$ fm^{-3} has been determined to be 231 ± 5 MeV from nuclear giant monopole resonances (GMR) [12] and the EOS at densities of $2\rho_0 < \rho < 5\rho_0$ has also been constrained by measurements of collective flows in nucleus-nucleus collisions [3].

Theoretical studies of the EOS of isospin asymmetric nuclear matter were started by Brueckner *et al.* [13] and Siemens [14] in the late 60 s. Since then, there have been many studies on this subject based on different many-body theories using various two-body and three-body forces or interaction Lagrangians. These many-body theories provide very useful tools for understanding the properties of hot and dense nuclear matter, and they can be roughly classified into three categories: the microscopic many-body approach, the effective-field theory approach, and the phenomenological approach. In the microscopic many-body approach, the nuclear many-body problem is treated microscopically using nucleon-nucleon interactions fitted to high-precision experimental data and is thus free of parameters. The microscopic many-body approach mainly includes the non-relativistic Brueckner-Hartree-Fock (BHF) approach [15−18], relativistic Dirac-Brueckner-Hartree-Fock (DBHF) approach [19−27], self-consistent Green's function approach [10, 28−31], and variational many-body approach [32−36]. In the effective-field theory approach, an effective interaction is constructed based on the effective-field theory (EFT), leading to a systematic expansion of the EOS in powers of density (the Fermi momentum). The effective-field theory approach can be based on the density functional theory [37, 38] or on chiral perturbation theory [39−44]. Since this approach can be linked to low energy QCD and its symmetry breaking, it has the advantage of having a small number of free parameters and a correspondingly higher predictive power. The phenomenological approach is based on effective density-dependent nuclear forces or effective interaction Lagrangians. In these approaches, a number of parameters have to be adjusted to fit the properties of many nuclei. These type of models mainly include the relativistic mean-field (RMF) theory [21, 45−53], relativistic and non-relativistic Hartree-Fock [54−65] or Thomas-Fermi approximations [64, 66−68]. These phenomenological approaches allow the most precise description for the properties of finite nuclei. Both the phenomenological and EFT approaches contain parameters that are fixed by nuclear properties around the saturation density and thus usually give excellent descriptions for the nuclear properties around or below the saturation density. Their predictions at the high density region are, however, probably unreliable. In addition, due to different approximations or techniques used in different microscopic many-body approaches, their predictions on the properties of nuclear matter could be very different even for the same bare nucleon-nucleon interaction [10, 69]. In particular, predictions on the properties of isospin asymmetric nuclear matter, especially the density dependence of the nuclear symmetry energy, are still significantly different for different many-body theory approaches.

Fortunately, heavy-ion reactions induced by radioactive beams provide a unique opportunity to investigate in terrestrial laboratories the EOS of asymmetric nuclear matter, particularly the density dependence of the nuclear symmetry energy. During the past decade, a large amount of theoretical and experimental efforts have been devoted to the study of the properties of isospin asymmetric nuclear matter via heavy-ion reactions [1, 2, 5, 70−113]. To extract information about the EOS of neutron-rich matter, especially the density dependence of the nuclear symmetry energy, from heavy-ion reactions induced by radioactive beams, one needs reliable theoretical tools. Transport models that include explicit isospin-dependent degrees of freedom are especially useful for understanding the role of isospin degree of freedom in the dynamics of central nuclear reactions induced by neutron nuclei at intermediate and high energies and in extracting information about the EOS of produced neutron-rich matter. During the past two decades, significant progresses have been made in developing semi-classical transport models for nuclear reactions. These semi-classical models mainly include the following two types: the Boltzmann-Uehling-Ulenbeck (BUU) model [114] and the quantum molecular dynamical (QMD) model [115]. While it is important to develop practically implementable quantum transport theories, applications of the semi-classical transport models have enabled us to learn a great deal of interesting physics from heavy-ion reactions. In particular, with the development of the radioactive nuclear beam physics, some isospin-dependent transport models [70−72, 75, 76, 101, 104, 116] have been successfully developed in recent years to describe the nuclear reactions induced by neutron nuclei at intermediate and high energies.

In studying the properties of asymmetric nuclear matter from heavy-ion reactions induced by neutron-rich nuclei, a key task is to identify experimental observables that are sensitive to the density dependence of the nuclear symmetry energy, especially at high densities. Because of the fact that the symmetry potentials for neutrons and protons have opposite signs and that they are generally weaker than the nu-

clear isoscalar potential at same density, most observables proposed so far use differences or ratios of isospin multiplets of baryons, mirror nuclei and mesons, such as the neutron/proton ratio of nucleon emissions [72], neutron-proton differential flow [86], neutron-proton correlation function [90, 91], $t/^3$He [92, 93, 104], π^-/π^+ [88, 89, 102, 108, 109], Σ^-/Σ^+ [105] and K^0/K^+ ratios [110, 111], etc. In addition, in order to reduce the systematical errors, multiple probes taken from several reaction systems using different isotopes of the same element have also been proposed. These multiple probes mainly include double ratio or double differential flow.

Indeed, recent experimental and theoretical analysis of the isospin diffusion data from heavy-ion reactions has led to significant progress in determining the nuclear symmetry energy at subnormal densities [116−118]. Based on the same underlying Skyrme interactions as the ones constrained by the isospin diffusion data, the neutron-skin thickness in ^{208}Pb calculated within the Hartree-Fock approach is consistent with available experimental data [119−121]. This symmetry energy is also consistent with that from a relativistic mean-field model using an accurately calibrated parameter set that reproduces both the giant monopole resonance in ^{90}Zr and ^{208}Pb, and the isovector giant dipole resonance of ^{208}Pb [122]. It further agrees with the symmetry energy recently obtained from isoscaling analyses of isotope ratios in intermediate-energy heavy ion collisions [123]. These different studies have provided so far the best phenomenological constraints on the symmetry energy at sub-normal densities. Information on the symmetry energy at supra-normal densities, on the other hand, remains inclusive and more efforts are needed to investigate the supra-normal density behavior of the symmetry energy. Heavy-ion collisions induced by future high energy radioactive beams that will be available at high energy radioactive beam facilities will provide a unique opportunity for determining the symmetry energy at supra-normal densities.

In the present paper, we review recent progress on the determination of the nuclear symmetry energy in heavy-ion reactions induced by neutron-rich nuclei. In particular, we review the exciting results on density dependence of the nuclear symmetry energy at subnormal densities determined from recent analysis of the isospin diffusion data in heavy-ion reactions. We also discuss the implications derived from this new information on nuclear effective interactions and the neutron skin thickness of heavy nuclei. In addition, we review theoretical progress in studying the behavior of nuclear symmetry energy at high density from heavy-ion reactions induced by high energy radioactive beams.

The paper is organized as follows. In Section 2, we give a brief introduction to the nuclear symmetry energy. We then describe in Section 3 the IBUU04 hadron transport model for nuclear reactions induced by radioactive beams at intermediate energies. In Section 4, we present the results from the IBUU04 model analysis of the isospin diffusion data in heavy-ion reactions and discuss the stringent constraint they have imposed on the nuclear symmetry energy around the nuclear matter saturation density. Based on the constrained symmetry energy from the isospin diffusion data, we discuss in Section 5 the implications of the isospin diffusion data on nuclear effective interactions and the neutron skin thickness of heavy nuclei. In Section 6, we review theoretical progress on studying the behavior of the nuclear symmetry energy at high density in heavy-ion reactions induced by high energy radioactive beams. Finally, a summary is given in Section 7.

2 The nuclear symmetry energy

In the parabolic approximation that has been verified by all many-body theories to date, the EOS of isospin asymmetric nuclear matter can be written as

$$E(\rho,\delta) = E(\rho,\delta=0) + E_{\rm sym}(\rho)\delta^2 + O(\delta^4) \quad (1)$$

where $\rho = \rho_{\rm n} + \rho_{\rm p}$ is the baryon density with $\rho_{\rm n}$ and $\rho_{\rm p}$ denoting the neutron and proton densities, respectively; $\delta = (\rho_{\rm n} - \rho_{\rm p})/(\rho_{\rm p} + \rho_{\rm n})$ is the isospin asymmetry; $E(\rho,\delta=0)$ is the energy per nucleon in symmetric nuclear matter, and

$$E_{\rm sym}(\rho) = \frac{1}{2}\frac{\partial^2 E(\rho,\delta)}{\partial\delta^2}|_{\delta=0} \quad (2)$$

is the nuclear symmetry energy. In Eq. (1), there are no odd-order δ terms due to the exchange symmetry of the proton and neutron in the nuclear matter (the charge symmetry of nuclear forces). Higher-order terms in δ are negligible. For example, the magnitude of the δ^4 term at ρ_0 has been estimated to be less than 1 MeV [14, 15, 33]. As a good approximation, the density-dependent symmetry energy $E_{\rm sym}(\rho)$ can thus be extracted from $E_{\rm sym}(\rho) \approx E(\rho,\delta=1) - E(\rho,\delta=0)$ which implies that the symmetry energy $E_{\rm sym}(\rho)$ is the energy cost to convert all protons in a symmetric nuclear matter to neutrons at the fixed density ρ.

Around the nuclear matter saturation density ρ_0, the nuclear symmetry energy $E_{\rm sym}(\rho)$ can be further expanded to second-order as

$$E_{\rm sym}(\rho) = E_{\rm sym}(\rho_0) + \frac{L}{3}\cdot\frac{\rho-\rho_0}{\rho_0} + \frac{K_{\rm sym}}{18}\left(\frac{\rho-\rho_0}{\rho_0}\right)^2 \quad (3)$$

where L and $K_{\rm sym}$ are the slope and curvature parameters of the nuclear symmetry energy at ρ_0, i.e.,

$$L = 3\rho_0 \frac{\partial E_{\rm sym}(\rho)}{\partial \rho}|_{\rho=\rho_0} \tag{4}$$

$$K_{\rm sym} = 9\rho_0^2 \frac{\partial^2 E_{\rm sym}(\rho)}{\partial^2 \rho}|_{\rho=\rho_0} \tag{5}$$

The L and $K_{\rm sym}$ characterize the density dependence of the nuclear symmetry energy around normal nuclear matter density, and thus provide important information on properties of the nuclear symmetry energy at both high and low densities.

At the nuclear matter saturation density ρ_0 and around $\delta = 0$, the isobaric incompressibility of asymmetric nuclear matter can be further expressed as [59, 124]:

$$K(\delta) = K_0 + K_{\rm asy}\delta^2 \tag{6}$$

where K_0 is the incompressibility of symmetric nuclear matter at the nuclear matter saturation density ρ_0 and the isospin-dependent part $K_{\rm asy} \approx K_{\rm sym} - 6L$ [83] characterizes the density dependence of the nuclear symmetry energy. In principle, the information on $K_{\rm asy}$ can be extracted experimentally by measuring the GMR of neutron-rich nuclei and a constraint of -566 ± 1350 MeV $< K_{\rm asy} <$ 139 ± 1617 MeV has been extracted earlier from a systematic study on the GMR of finite nuclei depending on the mass region of nuclei and the number of parameters used in parameterizing the incompressibility of finite nuclei [11]. The large uncertainties in the extracted $K_{\rm asy}$ thus does not allow us to distinguish the different nuclear symmetry energies in theoretical models.

Information about the nuclear symmetry energy is important not only for nuclear physics, but also for a number of important issues in astrophysics. For example, the prompt shock invoked to understand the explosion mechanism of a type II supernova requires a relatively soft EOS [125], which can be understood in terms of the dependence of the nuclear incompressibility on isospin. In the model for prompt explosion [126], the electron-capture reaction drives the star in the latest stage of collapse to an equilibrium state where the proton concentration is about $1/3$, which, according to microscopic many-body calculations, reduces the nuclear matter incompressibility by about 30% compared to that for symmetric nuclear matter. Moreover, the magnitude of proton concentration at β equilibrium in a neutron star is almost entirely determined by the symmetry energy. The proton fraction affects not only the stiffness of the EOS but also the cooling mechanisms of neutron stars [127, 128] and the possibility of kaon condensation ($e^- \to K^-\nu_e$) in dense stellar matter [129]. If the proton concentration is larger than a critical value of about 15%, the direct URCA process ($n \to p + e^- + \bar{\nu}_e,\ p + e^- \to n + \nu_e$) becomes possible, and would then enhance the emission of neutrinos, making it a more important process in the cooling of a neutron star [127].

Unfortunately, the density dependence of $E_{\rm sym}(\rho)$, especially its high density behavior, is poorly known and is regarded as the most uncertain among all properties of an isospin asymmetric nuclear matter. Even around the saturation density, values of the parameters L, $K_{\rm sym}$, and $K_{\rm asy}$ are still very uncertain with different theoretical models giving very different predictions. This can be seen in Fig. 1 where we show the density dependence of the nuclear symmetry energy from some of the most widely used microscopic many-body theories [10]. One sees that the theoretical predictions diverge widely at both low and high densities. In fact, even the sign of the symmetry energy above $3\rho_0$ is uncertain [9]. The theoretical uncertainties are largely due to a lack of knowledge about the isospin dependence of nuclear effective interactions and the limitations in the techniques in solving the nuclear many-body problem.

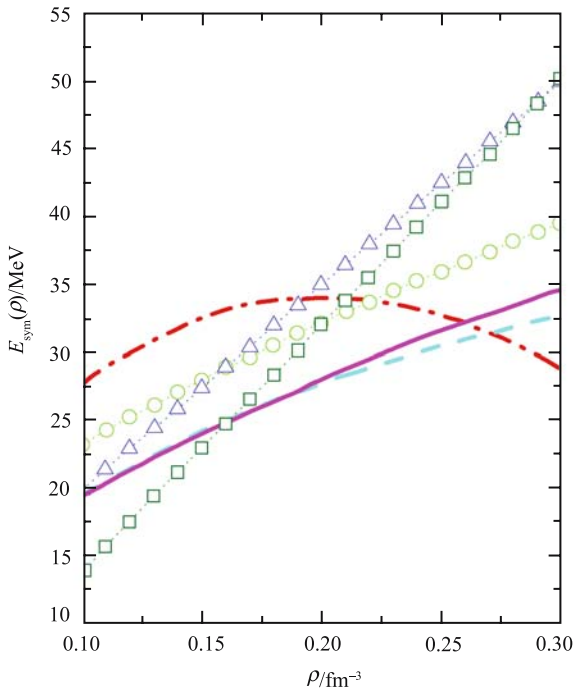

Fig.1 (*Color online*) Density dependence of the symmetry energy from the continuous choice Brueckner-Hartree-Fock with Reid93 potential (*circles*), self-consistent Green's function theory with Reid93 potential (*full line*), variational calculation with Argonne Av14 potential (*dashed line*), Dirac-Brueckner-Hartree-Fock calculation (*triangles*), relativistic mean-field model (*squares*), and effective field theory (*dash-dotted line*). Data are taken from Ref. [10].

As mentioned in the Introduction, heavy-ion reactions, es-

pecially those induced by radioactive beams, provide a unique opportunity to pin down the density dependence of nuclear symmetry energy in terrestrial laboratories. Indeed, significant progress has been made recently both experimentally and theoretically in determining the symmetry energy at subnormal densities. At sub-normal densities, a density-dependent symmetry energy of $E_{\rm sym}(\rho) \approx 31.6(\rho/\rho_0)^{0.69}$ has been found to best reproduce both the isospin diffusion [116−119, 121] and isoscaling [123] data in heavy-ion collisions as well as the presently acceptable neutron-skin thickness in ^{208}Pb [119−121]. Together, these results represent the best phenomenological constraints available so far on the symmetry energy at sub-normal densities. Although the high density behavior of the symmetry energy remains largely undetermined, future high energy radioactive beams that will be available at high energy radioactive beam facilities will allow us to determine the symmetry energy at supra-normal densities.

3 IBUU transport model for nuclear reactions induced by radioactive beams

Transport models are useful theoretical tools not only for studying the reaction mechanisms but also for extracting information on the properties of produced hot dense matter in heavy ion collisions. For nuclear reactions induced by radioactive beams, comparing experimental data with transport model calculations allows us to extract the information about the EOS of neutron-rich matter. The IBUU model, which has been very useful in understanding a number of new phenomena associated with the isospin degree of freedom in heavy-ion reactions, is an isospin- and momentum-dependent transport model that is based on the Boltzmann-Uhling-Uhlenbeck equation and is applicable for heavy-ion reactions induced by both stable and radioactive beams [97, 98].

In the IBUU model, besides nucleons, Δ and N^* resonances as well as pions and their isospin-dependent dynamics are included. The initial neutron and proton density distributions of projectile and target nuclei are obtained from the Relativistic Mean-field model or the Skyrme-Hartree-Fock model. It has the option of using either the experimental free-space nucleon-nucleon (NN) scattering cross-sections or the in-medium NN cross-sections. For NN inelastic collisions, the experimental free-space cross-sections are used scince as their in-medium cross-sections are still very much controversial. The total and differential cross-sections for all other particles are taken either from experimental data or obtained by using the detailed-balance formula. Time dependence of the isospin-dependent phase-space distribution functions of involved particles are solved numerically using the test-particle method. In treating NN scattering, the isospin dependent Pauli blocking factors for fermions is also included.

In the following, we outline the two major ingredients, i.e., the single-nucleon potential and the NN cross-sections, of the version IBUU04 of the isospin- and momentum-dependent IBUU transport model for nuclear reactions induced by radioactive beams [97, 98]. Other details, such as the initialization of the phase space distributions of colliding nuclei and the Pauli blocking, *etc.* can be found in Refs. [1, 2, 72, 97, 98, 116].

3.1 Single-nucleon potential

One of the most important inputs to all transport models is the single-nucleon potential. Both the isovector (symmetry potential) and isoscalar parts of this potential should be momentum-dependent due to the non-locality of strong interactions and the Pauli exchange effects in many-fermion systems. In the IBUU04, we use a single-nucleon potential derived from the Hartree-Fock approximation based on a modified Gogny effective interaction (MDI) [130], i.e.,

$$\begin{aligned} U(\rho,\delta,\boldsymbol{p},\tau,x) = {} & A_u(x)\frac{\rho_{\tau'}}{\rho_0} + A_l(x)\frac{\rho_\tau}{\rho_0} \\ & + B(\frac{\rho}{\rho_0})^\sigma(1-x\delta^2) - 8\tau x\frac{B}{\sigma+1}\frac{\rho^{\sigma-1}}{\rho_0^\sigma}\delta\rho_{\tau'} \\ & + \frac{2C_{\tau,\tau}}{\rho_0}\int \mathrm{d}^3p'\frac{f_\tau(\boldsymbol{r},\boldsymbol{p}')}{1+(\boldsymbol{p}-\boldsymbol{p}')^2/\Lambda^2} \\ & + \frac{2C_{\tau,\tau'}}{\rho_0}\int \mathrm{d}^3p'\frac{f_{\tau'}(\boldsymbol{r},\boldsymbol{p}')}{1+(\boldsymbol{p}-\boldsymbol{p}')^2/\Lambda^2} \end{aligned} \quad (7)$$

In the above $\tau = 1/2$ $(-1/2)$ for neutrons (protons) and $\tau \neq \tau'$; $\sigma = 4/3$; $f_\tau(\boldsymbol{r},\boldsymbol{p})$ is the phase space distribution function at coordinate $\boldsymbol{r}$ and momentum $\boldsymbol{p}$. The parameters $A_u(x), A_l(x), B, C_{\tau,\tau}, C_{\tau,\tau'}$ and Λ were obtained by fitting the momentum dependence of $U(\rho,\delta,\boldsymbol{p},\tau,x)$ to that predicted by the Gogny Hartree-Fock and/or the Brueckner-Hartree-Fock calculations, the saturation properties of symmetric nuclear matter, and the symmetry energy of 31.6 MeV at normal nuclear matter density $\rho_0 = 0.16$ fm^{-3}[130]. The incompressibility K_0 of symmetric nuclear matter at ρ_0 is set to be 211 MeV. The parameters $A_u(x)$ and $A_l(x)$, given by

$$A_u(x) = -95.98 - x\frac{2B}{\sigma+1}, \quad A_l(x) = -120.57 + x\frac{2B}{\sigma+1} \quad (8)$$

depend on the parameter x that can be adjusted to mimic the predicted $E_{\rm sym}(\rho)$ from microscopic and/or phenomenological many-body theories. The last two terms in Eq. (7) contain the momentum-dependence of the single-particle potential. The momentum dependence of the symmetry potential

stems from the different interaction strength parameters $C_{\tau,\tau'}$ and $C_{\tau,\tau}$ for a nucleon of isospin τ interacting, respectively, with unlike and like nucleons in the background fields. More specifically, we use $C_{\tau,\tau'} = -103.4$ MeV and $C_{\tau,\tau} = -11.7$ MeV. With these parameters, the isoscalar potential estimated from $(U_{\rm neutron}+U_{\rm proton})/2$ agrees reasonably well with predictions from the variational many-body theory [131], the more advanced BHF approach [132] including three-body forces, and the Dirac-Brueckner-Hartree-Fock (DBHF) calculations [27] in a broad range of density and momentum. As an example, we show in Fig. 2 the density dependence of the symmetry energy for $x = -2$, -1, 0 and 1. It is seen that the symmetry energy becomes softer with increasing value of the parameter x.

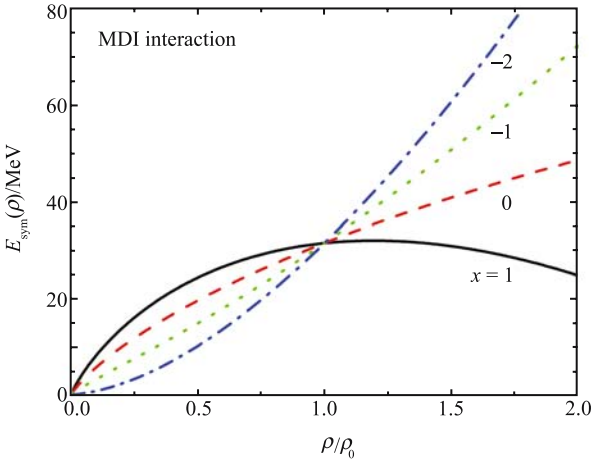

Fig.2 (*Color online*) Symmetry energy as a function of density for the MDI interaction with $x = 1, 0, -1$ and -2. Taken from Ref. [118].

The interaction part of nuclear symmetry energy can be parameterized by

$$E_{\rm sym}^{\rm pot}(\rho) = F(x)\rho/\rho_0 + [18.6 - F(x)](\rho/\rho_0)^{G(x)} \qquad (9)$$

with $F(x)$ and $G(x)$ given in Table 1 for $x = 1$, 0, -1 and -2. Also shown in Table 1 are other properties of the symmetry energy, including its slope parameter L and curvature parameter $K_{\rm sym}$ at ρ_0, as well as the isospin-dependent part $K_{\rm asy}$ of the isobaric incompressibility of asymmetric nuclear matter. It is seen that the stiffness of the symmetry energy increases with decreasing x values.

What is particularly interesting and important for nuclear reactions induced by neutron-rich nuclei is the isovector (symmetry) potential. The strength of this potential can be estimated very accurately from $(U_{\rm neutron} - U_{\rm proton})/2\delta$ [97, 98]. In Fig. 3, the strength of the symmetry potential for four x parameters is displayed as a function of momentum and density. Here we have only plotted the symmetry potential at

Table 1 The parameters F(MeV), G, $K_{\rm sym}$(MeV), L (MeV), and $K_{\rm asy}$ (MeV) for different values of x. Taken from Ref. [118].

x	F	G	$K_{\rm sym}$	L	$K_{\rm asy}$
1	107.232	1.246	−270.4	16.4	−368.8
0	129.981	1.059	−88.6	62.1	−461.2
−1	3.673	1.569	94.1	107.4	−550.3
−2	−38.395	1.416	276.3	153.0	−641.7

sub-saturation densities most relevant to heavy-ion reactions studies at intermediate energies. The momentum dependence of the symmetry potential is seen to be the same for all values of x as the parameter x appears by construction only in the density-dependent part of the single-nucleon potential given by Eq.(7). Systematic analysis of a large number of nucleon-nucleus scattering experiments and (p,n) charge exchange reactions at beam energies below about 100 MeV has shown that the data can be well described by the parametrization $U_{\rm Lane} = a - bE_{\rm kin}$ with $a \approx 22 - 34$ MeV and $b \approx 0.1 - 0.2$ [133−136]. Although the uncertainties in both parameters a and b are large, the symmetry potential at ρ_0, i.e., the Lane potential, clearly decreases approximately linearly with increasing beam energy $E_{\rm kin}$. This provides a stringent constraint on the symmetry potential. The potential in Eq. (7) at ρ_0 satisfies this requirement very well as seen in Fig. 3. This can be more clearly seen from the solid line in Fig. 4 which gives the kinetic energy dependence of $(U_{\rm neutron} - U_{\rm proton})/2\delta$ at normal nuclear saturation density given by the MDI interaction with $x = 0$. Also shown in this figure are the predicted kinetic energy dependence of the symmetry potential from the MDI interaction with $x = 0$ for densities away from normal nuclear density, which are presently not known empirically. Experimental determination of both the density and momentum dependence of the symmetry potential is thus of great interest, and heavy-ion reactions with radioactive beams provides a unique tool to explore this information in terrestrial laboratories.

Although the effective mass of a nucleon in nuclear matter depends on the density of nuclear matter as well as the momentum of the nucleon [24, 137, 138], the momentum dependence of the symmetry potential further leads to different effective masses for neutrons and protons in isospin asymmetric nuclear matter, i.e.,

$$\frac{m_\tau^*}{m_\tau} = \left\{1 + \frac{m_\tau}{p}\frac{{\rm d}U_\tau}{{\rm d}p}\right\} \qquad (10)$$

When the effective mass is evaluated at the Fermi momentum $p_\tau = p_{\rm f}(\tau)$, Eq. (10) yields the Landau mass which is related to the f_1 Landau parameter of a Fermi liquid [24, 137, 138]. A detailed discussion about different kinds of effective masses can be found in Ref. [137]. With the potential in

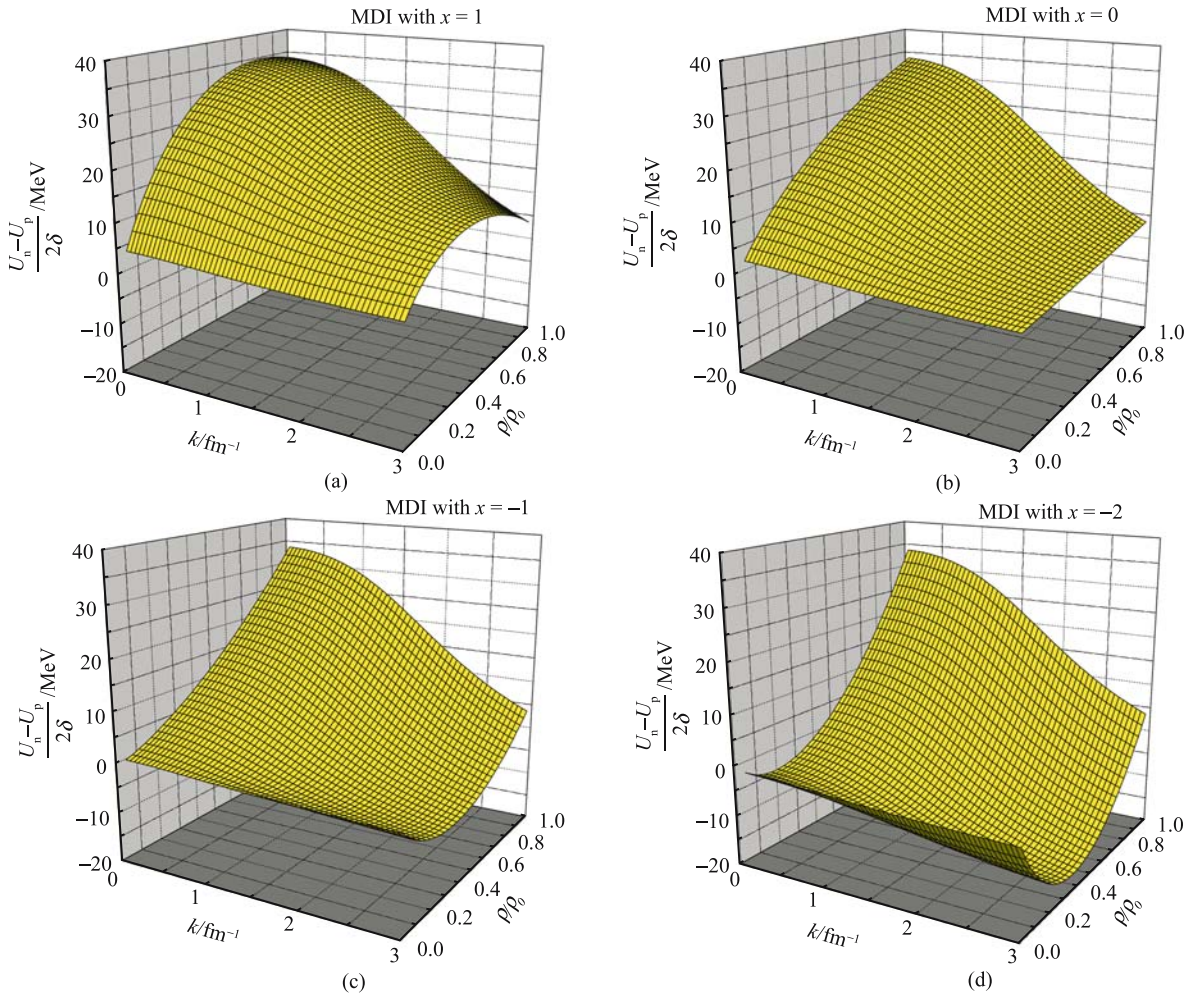

Fig.3 (*Color online*) Symmetry potential as a function of momentum and density for MDI interactions with $x = 1$ **(a)**, $x = 0$ **(b)**, $x = -1$ **(c)** and $x = -2$ **(d)**. Taken from Ref. [116].

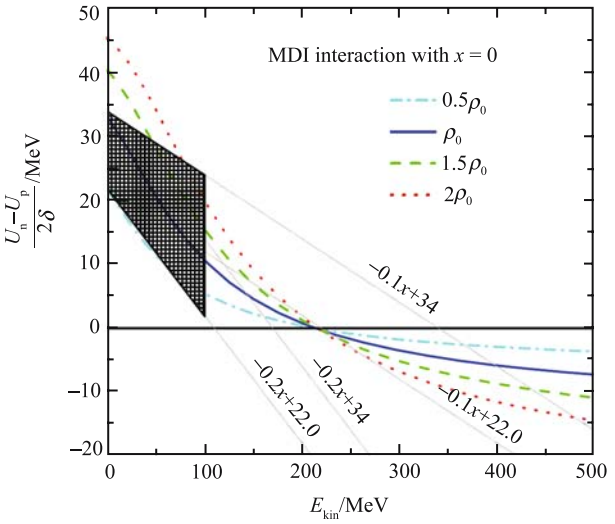

Fig.4 (*Color online*) Kinetic energy dependence of $(U_{\rm neutron}-U_{\rm proton})/2\delta$ at different densities using the MDI interaction with $x = 0$. The shaded region indicates the experimental constraint.

Eq. (7), the nucleon effective masses are independent of the x parameter as the momentum-dependent part of the nuclear potential is independent of the parameter x.

Shown in Fig. 5 are the effective masses of neutrons and protons at their respective Fermi surfaces as functions of density [Fig.5(a)] and isospin asymmetry [Fig.5(b)] obtained from the MDI interaction. It is seen that the effective mass of neutrons is larger than that of protons and the splitting between them increases with both the density and isospin asymmetry of the medium. Although the momentum dependence of the symmetry potential and the associated splitting between the neutron and proton effective masses are still highly controversial among different approaches and/or using different nuclear effective interactions [101, 139, 140], the results presented here are consistent with the predictions from all non-relativistic microscopic models, see, e.g., [17, 132, 141], and the non-relativistic limit of microscopic relativistic many-body theories, see, e.g., [24−27]. Recent transport

model studies have indicated that the neutron/proton ratio at high transverse momenta and/or rapidities is a potentially useful probe of the splitting between the neutron and proton effective masses in neutron-rich matter [5, 97, 98].

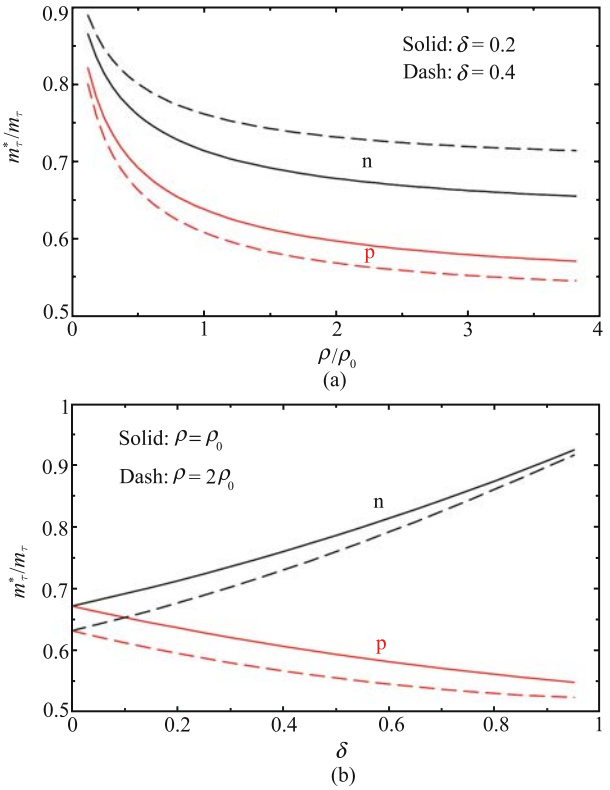

Fig.5 (*Color online*) Neutron and proton effective masses in asymmetric matter as a function of density **(a)** and isospin asymmetry **(b)**. Taken from Ref. [116].

The effect due to the momentum dependence of nuclear mean-field potential can be studied by comparing its predictions with those obtained using the momentum-independent nucleon potential $U(\rho,\delta,\tau) \equiv U_0(\rho) + U_{\rm sym}^{\rm MDI(x)}(\rho,\delta,\tau)$ with the isoscalar part $U_0(\rho)$ taken from the original momentum-independent soft nuclear potential with $K_0 = 200$ MeV (SBKD) introduced by Bertsch, Kruse and Das Gupta [142], i.e.,

$$U_{\rm SBKD}(\rho) = -356\rho/\rho_0 + 303(\rho/\rho_0)^{7/6} \tag{11}$$

For the momentum-independent symmetry potential $U_{\rm sym}^{\rm MDI}(x)(\rho,\delta,\tau)$, it can be obtained from $U_{\rm sym}^{\rm MDI(x)}(\rho,\delta,\tau) = \partial W_{\rm sym}/\partial\rho_\tau$ using the isospin-dependent part of the potential energy density $W_{\rm sym} = E_{\rm sym}^{\rm pot}(\rho)\cdot\rho\cdot\delta^2$ where $E_{\rm sym}^{\rm pot}(\rho)$ is given by Eq. (9) from the MDI interaction. Therefore, the momentum-independent SBKD potential that has $K_0 = 200$ MeV [142] and exactly the same $E_{\rm sym}(\rho)$ as the MDI interaction is

$$\begin{aligned} U_{\rm SBKD}(\rho,\delta,\tau) = &-356\,\rho/\rho_0 + 303\,(\rho/\rho_0)^{7/6} \\ &+ 4\tau E_{\rm sym}^{\rm pot}(\rho) + [18.6 - F(x)] \\ &\times [G(x)-1](\rho/\rho_0)^{G(x)}\delta^2 \end{aligned} \tag{12}$$

3.2 In-medium nucleon-nucleon cross-sections

Another important quantity in the IBUU model are the in-medium NN cross-sections. While much attention has been given to finding experimental observables that can constrain the symmetry energy, little effort has been made so far to study the NN cross-sections in isospin asymmetric nuclear matter. Most of existing works on in-medium NN cross-sections have concentrated on their density dependence in isospin symmetric nuclear matter, see, e.g., [143−152]. One simple model for in-medium NN cross-sections is the effective mass scaling model [143, 144, 147]. In this model, while both the incoming current in the initial state and the level density of the final state in an NN scattering depend on the effective masses of colliding nucleons, the scattering matrix elements are assumed to be the same in free-space and in the medium. As a result, the ratio of the NN cross-section in nuclear medium $\sigma_{\rm NN}^{\rm medium}$ to that in free-space value $\sigma_{\rm NN}^{\rm free}$ is simply given by

$$R_{\rm medium} \equiv \sigma_{\rm NN}^{\rm medium}/\sigma_{\rm NN}^{\rm free} = (\mu_{\rm NN}^*/\mu_{\rm NN})^2 \tag{13}$$

where $\mu_{\rm NN}$ and $\mu_{\rm NN}^*$ are the reduced masses of scattering nucleon pairs in free-space and in the medium, respectively. Since the nucleon mass becomes smaller in nuclear medium, the in-medium NN cross-section is smaller than its value in free space. The relation given in Eq. (13) was recently found to be consistent with calculations based on the DBHF theory [153] for nucleon pairs with relative momenta less than about 240 MeV/c and in nuclear matter with densities less than about $2\rho_0$. This finding thus lends a strong support to the effective mass scaling model of in-medium NN cross-sections in this limited density and momentum ranges. We have thus extended this model to determine the in-medium NN cross-sections in the asymmetric nuclear matter produced in nuclear reactions induced by radioactive beams. For nucleon-nucleon scatterings at higher energies, inelastic reaction channels become important. Although there were some studies on in-medium effects in these channels [154−157], the experimental free-space cross-sections are used in the IBUU model as the model is mainly for heavy-ion collisions at intermediate energies where NN inelastic scatterings are less important than elastic scatterings.

While the effective masses and the in-medium NN cross-sections have to be calculated dynamically in the evolving

environment created during heavy-ion reactions, it is instructive to examine the in-medium NN cross-sections in isospin asymmetric nuclear matter at zero temperature. In this situation, the integrals in Eq. (7) can be analytically carried out. Specifically, it is given by [130, 158]

$$\int \mathrm{d}^3p' \frac{f_\tau(\boldsymbol{r},\boldsymbol{p}')}{1+(\boldsymbol{p}-\boldsymbol{p}')^2/\Lambda^2} = \frac{2}{h^3}\pi\Lambda^3\left[\frac{p_{\mathrm{f}}^2(\tau)+\Lambda^2-p^2}{2p\Lambda}\ln\frac{[p+p_{\mathrm{f}}(\tau)]^2+\Lambda^2}{[p-p_{\mathrm{f}}(\tau)]^2+\Lambda^2} + \frac{2p_{\mathrm{f}}(\tau)}{\Lambda}-2\arctan\frac{p+p_{\mathrm{f}}(\tau)}{\Lambda}-2\arctan\frac{p-p_{\mathrm{f}}(\tau)}{\Lambda}\right] \quad (14)$$

The reduction factor R_{medium} for in-medium NN cross sections can thus also be obtained analytically, albeit lengthy.

As an illustration, we show in Fig. 6 the reduction factor R_{medium} for a simplified case of two colliding nucleons having the same momentum p. The R_{medium} factor is examined as a function of density [Fig.6(a)], isospin asymmetry [Fig.6(b)] and the momentum [Fig.6(c)]. It is interesting to note that not only are in-medium NN cross-sections reduced compared with their free-space values but also the nn and pp cross-sections become different while their free-space cross-sections are the same. Moreover, the difference between the nn and pp scattering cross sections grows in more asymmetric matter. The larger in-medium cross sections for nn than for pp are completely due to the positive neutron-proton effective mass splitting with the effective interaction used. This feature may serve as a probe of the neutron-proton effective mass splitting in neutron-rich matter. We also note that in-medium NN cross-sections are also independent of the parameter x as they are solely determined by the momentum dependence of the nuclear potential used in the model.

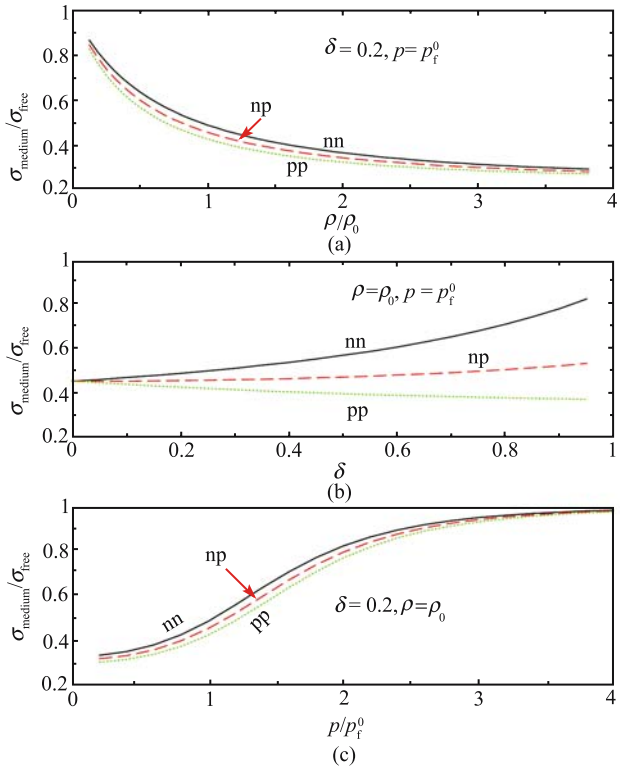

Fig.6 (*Color online*) The reduction factor of the in-medium nucleon-nucleon cross-sections compared to their free-space values as a function of density **(a)**, isospin asymmetry **(b)** and momentum **(c)**. Taken from Ref. [116].

4 Constraining the symmetry energy at sub-normal densities using isospin diffusion data

The IBUU model outlined above has been used to study many observables in heavy-ion reactions induced by both stable and radioactive beams. In this section, we illustrate one of its applications in extracting the density dependence of nuclear symmetry energy from the isospin diffusion data in heavy-ion collisions.

Isospin diffusion in heavy-ion collisions has been shown to depend sensitively on the density dependence of nuclear symmetry energy [99, 100, 159]. Within a momentum-independent transport model, in which the nuclear potential depends only on local nuclear density, the isospin diffusion data from recent experiments at the NSCL/MSU (National Superconducting Cyclotron Laboratory at Michigan State University) was found to favor a quadratic density dependence for the interaction part of nuclear symmetry energy [117]. This conclusion has stimulated much interest because of its implications to nuclear many-body theories and nuclear astrophysics. However, the nuclear potential acting on a nucleon is known to depend also on its momentum. For nuclear isoscalar potential, its momentum dependence is well-known and is important in extracting information about the equation-of-state of symmetric nuclear matter [3, 146, 160−166]. The momentum dependence of the isovector (symmetry) potential [9, 130, 135, 138] has also been shown to be important for understanding a number of isospin-related phenomena in heavy-ion reactions [96−98, 101]. It is therefore necessary to include momentum dependence in both isoscalar and isovector potentials for studying the effect of nuclear symmetry energy on isospin diffusion.

Isospin diffusion in heavy ion collisions can in principle be studied by examining the average isospin asymmetry of the projectile-like residue in the final state. Since reactions at intermediate energies are complicated by preequilibrium particle emission and production of neutron-rich fragments at mid-rapidity, differences of isospin diffusions in mixed and symmetric systems are usually used to minimize these effects

[117]. To study isospin diffusion in ^{124}Sn + ^{112}Sn reactions at $E = 50$ MeV/nucleon and an impact parameter of $b = 6$ fm, we thus also consider the reaction systems ^{124}Sn + ^{124}S and ^{112}Sn + ^{112}Sn and at the same energy and impact parameter as in Ref. [117]. The degree of isospin diffusion in the reaction ^{124}Sn + ^{112}Sn is then measured by [167]

$$R_i = \frac{2X_{^{124}\mathrm{Sn}+^{112}\mathrm{Sn}} - X_{^{124}\mathrm{Sn}+^{124}\mathrm{Sn}} - X_{^{112}\mathrm{Sn}+^{112}\mathrm{Sn}}}{X_{^{124}\mathrm{Sn}+^{124}\mathrm{Sn}} - X_{^{112}\mathrm{Sn}+^{112}\mathrm{Sn}}} \quad (15)$$

where X is the average isospin asymmetry $\langle\delta\rangle$ of the ^{124}Sn-like residue defined as the composition of nucleons with local densities higher than $\rho_0/20$ and velocities larger than $1/2$ the beam velocity in the c.m. frame. A density cut of $\rho_0/8$ is found to give almost the same results. In the ideal case, the value of R_i ranges between 0.05 and 1 from complete mixing to full transparency.

4.1 Effects of momentum-dependent interactions on isospin diffusion

Effects of momentum-dependent interactions on dynamics of heavy-ion collisions can be seen from the time evolution of the density distribution [96]. In Fig.7, we show the density contour $\rho(x, 0, z)$ in the reaction plane at different times for the reaction ^{124}Sn + ^{112}Sn at $E/A = 50$ MeV and $b = 6$ fm calculated with $x = -1$ using both the MDI and the soft Bertsch-Das Gupta-Kruse (SBKD) interactions. It should be noted that the former (MDI) interactions are momentum dependent for both isoscalar and isovector nuclear potentials while the latter (SBKD) interactions do not include any momentum dependence in either isoscalar or isovector nuclear potentials though both interactions have similar incompressibility K_0 and the same density dependence in the symmetry energy. The experimental free space NN cross-sections are used in these calculations. It is seen that both interactions give similar time evolution of the collisions dynamics, namely, projectile-like and target-like residues can be clearly separated after about 100 fm/c. Detailed examinations indicate, however, that the reaction system expands more quickly and there are also more emitted nucleons in the case of the momentum-dependent MDI interaction than that of the momentum-independent SBKD interaction.

In Fig. 8, we show the measured R_i together with the predictions from the IBUU04 for the time evolution of both R_i and the average central densities calculated with $x = -1$ using both the MDI and the soft SBKD interactions. It is seen that isospin diffusion occurs mainly from about 30 fm/c to 80 fm/c when average central density decreases from about $1.2\rho_0$ to $0.3\rho_0$. However, the value of R_i still changes slightly with time until after about 120 fm/c when projectile-like and target-like residues are well separated as shown in Fig. 7. This is partly due to the fact that the isovector potential remains appreciable at low density as shown in Fig.9, where the symmetry potential $(U_\mathrm{n} - U_\mathrm{p})/2\delta$ is shown as a function of

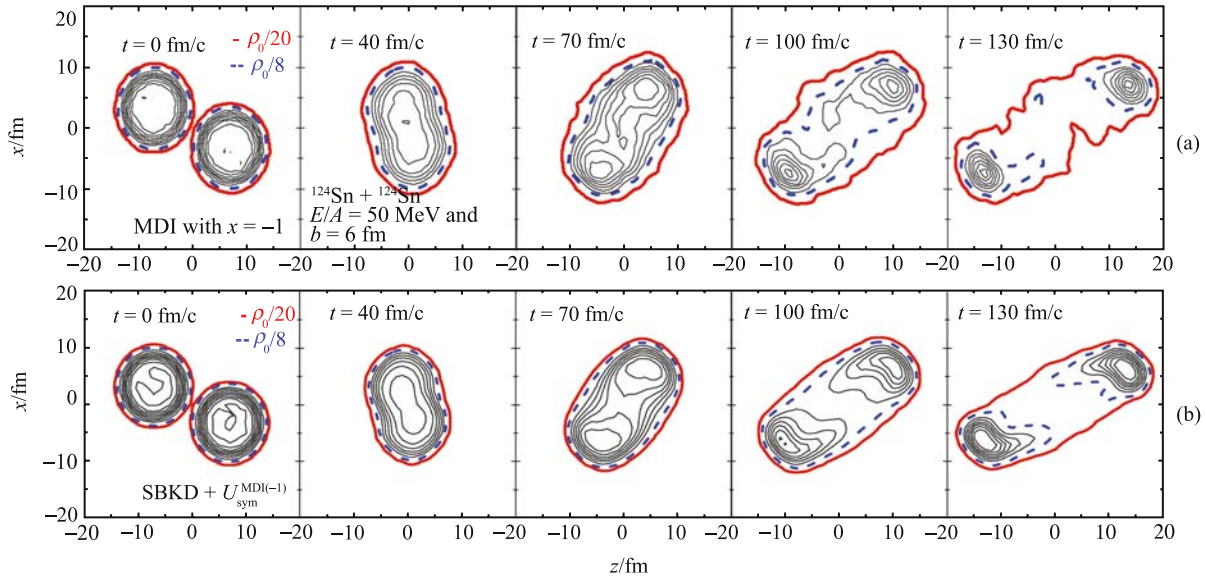

Fig.7 (*Color online*) Density contour $\rho(x, 0, z)$ in the reaction plane at different times for the reaction ^{124}Sn + ^{112}Sn at $E/A = 50$ MeV and $b = 6$ fm by using momentum-dependent interaction MDI with $x = -1$ **(a)** and momentum-independent interaction SBKD with momentum-independent symmetry potential $U_\mathrm{sym}^{\mathrm{MDI}(-1)}(\rho, \delta, \tau)$ **(b)**. Thick solid lines represent ρ_0/20 while dashed lines represent ρ_0/8.

nucleon momentum [panel (a)] or density [panel (b)] for the MDI interaction and as a function of density for the SBKD interaction [panel (c)]. Also, evaluating isospin diffusion R_i based on three reaction systems, which have different time evolutions for the projectile residue as a result of different total energies and numbers of nucleons, further contributes to the change of R_i at low density. For the two interactions consider here, the main difference between the values for R_i appears in the expansion phase when densities in the participant region are well below ρ_0. The experimental data from MSU are seen to be reproduced nicely by the MDI interaction with $x = -1$, while the SBKD interaction with $x = -1$ leads to a significantly lower value for R_i as the strength of the momentum-independent symmetry potential is stronger (see Fig. 9), which has been shown to enhance the isospin diffusion [100, 117, 159].

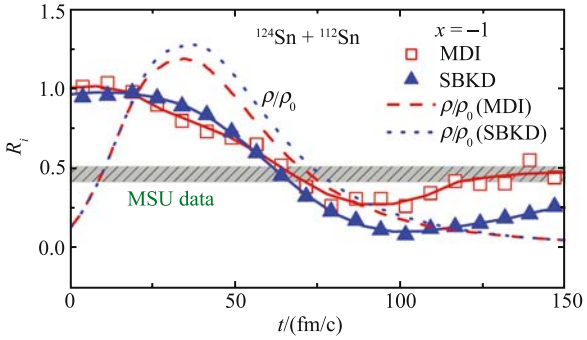

Fig.8 (*Color online*) Degree of isospin diffusion as a function of time with the MDI and SBKD interactions. Corresponding time evolutions of central density are also shown. Taken from Ref. [118].

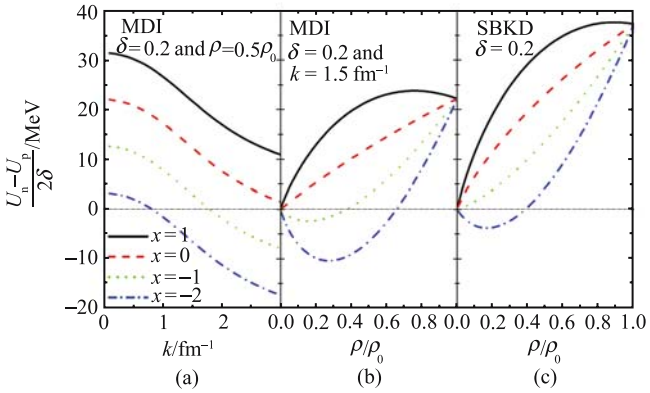

Fig.9 (*Color online*) Symmetry potential as a function of nucleon momentum **(a)** or density **(b)** with the MDI interaction and SBKD interaction **(c)**. Taken from Ref. [118].

Effects of the symmetry energy on isospin diffusion were also studied by varying the parameter x [118]. Shown in Fig.10 is the final saturated value for $1 - R_i$, which measures the degree of isospin diffusion, as a function of $K_{\rm asy}$ for both MDI and SBKD interactions. It is obtained by averaging the value of $1 - R_i$ after 120 fm/c with error bars corresponding to its dispersion, whose magnitude is similar to the error band shown in Ref. [117] for the theoretical results from the momentum-independent BUU model. For the SBKD interaction without momentum dependence, the isospin diffusion decreases monotonically (i.e., increasing value for R_i) with increasing strength of $K_{\rm asy}$ as the corresponding isovector potential is mostly positive and decreases with increasing stiffness of $E_{\rm sym}(\rho)$ in the whole range of the considered x parameter. The isospin diffusion is reduced when the momentum-dependent interaction MDI is used as the momentum dependence weakens the strength of symmetry potential except for $x = -2$. As seen in Fig. 9, the symmetry potential in the MDI interaction has the smallest strength for $x = -1$ as it is close to zero at $k \approx 1.5$ fm^{-1} and $\rho/\rho_0 \approx 0.5$, and increases again with further hardening of the symmetry energy, e.g., $x = -2$, when it becomes largely negative at all momenta and densities. The MDI interaction with $x = -1$ thus gives the smallest degree of isospin diffusion among the interactions considered here and reproduces the MSU data as already shown in Fig. 8.

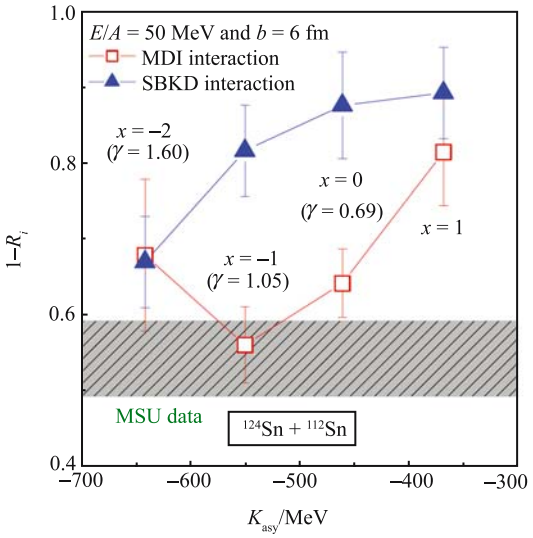

Fig.10 (*Color online*) Degree of isospin diffusion as a function of $K_{\rm asy}$ with the MDI and SBKD interactions. γ is the parameter for fitting the corresponding symmetry energy with $E_{\rm sym}(\rho) = 31.6(\rho/\rho_0)^{\gamma}$. Taken from Ref. [118].

The symmetry energy in the MDI interaction with $x = -1$ can be parameterized as $E_{\rm sym}(\rho) \approx 31.6(\rho/\rho_0)^{1.05}$. It leads to a value of $K_{\rm asy} \approx -550$ MeV for the isospin dependent

part of the isobaric incompressibility of asymmetric nuclear matter, which should be compared to the published constraint of -566 ± 1350 MeV $< K_{\rm asy} < 139 \pm 1617$ MeV extracted earlier from studying giant monopole resonances [11].

4.2 Effects of in-medium NN cross-sections on isospin diffusion

The isospin degree of freedom plays an important role in heavy-ion collisions through both the nuclear EOS and the NN scatterings [1, 2]. In particular, the transport of isospin asymmetry between two colliding nuclei is expected to depend on not only the symmetry potential through the density dependence of the symmetry energy $E_{\rm sym}(\rho)$ but also the in-medium NN cross-sections. The two are related, respectively, to the long-range and the short-range parts of the isospin-dependent in-medium nuclear effective interactions. For instance, the drifting contribution to the isospin transport in a nearly equilibrium system is proportional to the product of the mean relaxation time $\tau_{\rm np}$ and the isospin asymmetric force $F_{\rm np}$ [99]. While $F_{\rm np}$ is directly related to the gradient of the symmetry potential, $\tau_{\rm np}$ is inversely proportional to the neutron-proton (np) scattering cross-section $\sigma_{\rm np}$ [99]. Furthermore, the collisional contribution to the isospin transport in non-equilibrium systems is generally expected to be proportional to the np scattering cross-section. In the above study on isospin diffusion, the free-space NN cross-sections were used. In this section, we review the effects of in-medium NN cross sections on the isospin diffusion in heavy-ion collisions.

Shown in Fig. 11 is the time evolution of R_i re-calculated using the in-medium NN cross-sections and the MDI interaction with four x parameters. It is seen that the net isospin transport and the influence of the x parameter show up mainly in the expansion phase of the reaction after about 40 fm/c and become relatively stable after about 80 fm/c. In the late stage of the reaction, the values of R_i from $x = -1$ and 0 come close to the experimental data from MSU, which is shown by the shaded band.

For a more meaningful comparison with the experimental data, the time average of R_i between $t = 120$ fm/c and 150 fm/c has been used as in Fig. 8. Shown in Fig. 12 is a comparison of the average strength of isospin transport $1 - R_i$ obtained with the free and in-medium NN cross-sections, respectively, as a function of the asymmetric part of the isobaric incompressibility of nuclear matter at ρ_0, i.e., $K_{\rm asy}(\rho_0)$. The error bars were drawn to indicate fluctuations and were obtained from the dispersion in the time evolution of R_i [118]. First, it is interesting to note that with the in-medium NN

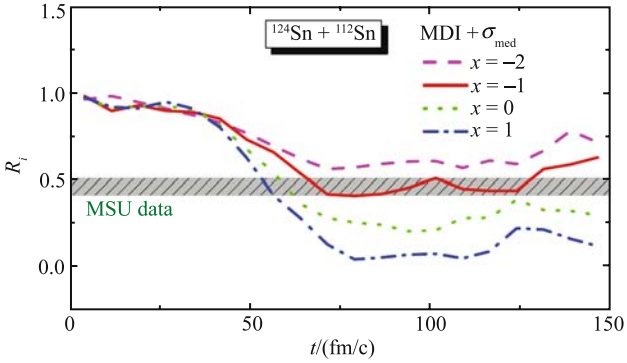

Fig.11 (*Color online*) Time evolution of the isospin diffusion R_i using MDI interactions with different x parameters and the in-medium nucleon-nucleon cross-sections. Taken from Ref. [116].

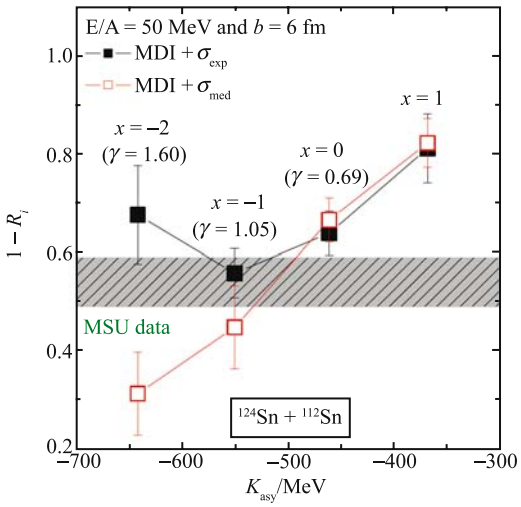

Fig.12 (*Color online*) Degree of isospin diffusion as a function of $K_{\rm asy}(\rho_0)$ with the free (*filled squares*) and in-medium (*open squares*) NN cross-sections. Taken from Ref. [116].

cross-sections the strength of isospin transport $1 - R_i$ decreases monotonically with decreasing value of x. With the free-space NN cross-sections, there appears, however, to be a minimum at around $x = -1$. Moreover, this minimum is the point closest to the experimental data. This allowed us to extract the value of $K_{\rm asy}(\rho_0) = -550 \pm 100$ MeV. With the in-medium NN cross-sections we can now further narrow down the $K_{\rm asy}(\rho_0)$ to be about -500 ± 50 MeV. The latter is consistent with that extracted from studying the isospin dependence of giant resonances of ^{112}Sn to ^{124}Sn isotopes by Fujiwara et al at Osaka [168]. Also shown in the figure are the γ values used in fitting the symmetry energy with $E_{\rm sym}(\rho) = 31.6(\rho/\rho_0)^{\gamma}$. The results with the in-medium NN cross-sections constrain the γ parameter to be between 0.69 and 1.05. The lower value is close to what is extracted from studying giant resonances [169, 170]. The value of $\gamma = 1.05$

extracted earlier using the free-space NN cross-sections sets an upper limit.

The difference in $1 - R_i$ obtained with the free-space and the in-medium NN cross-sections is small for $x = 1$ and $x = 0$, but becomes large for $x = -1$ and $x = -2$. The increasing effect of the in-medium NN cross-sections with decreasing $K_{\rm asy}(\rho_0)$ or x parameter can be understood from consideration of the contributions from the symmetry potential and the np scatterings. As we have mentioned above, both contributions to the isospin transport depend on the np scattering cross-section $\sigma_{\rm np}$. While the collisional contribution is proportional to the np scattering cross section $\sigma_{\rm np}$, the mean-field contribution is proportional to the product of the isospin asymmetric force $F_{\rm np}$ and the inverse of $\sigma_{\rm np}$. The overall effect of the in-medium NN cross-sections on isospin transport is a result of a complicated combination of both the mean field and the NN scatterings. Generally speaking, the symmetry potential effects on the isospin transport will become weaker when the NN cross-sections are larger, while the symmetry potential effects will show up more clearly if smaller NN cross-sections are used. This feature can be seen from Fig. 9. For $x = 1$ and $x = 0$, the symmetry potential and its gradient with respect to density, as shown in Fig. 9, are large at low densities where the majority of net isospin transport occurs. The $F_{\rm np}$ factor makes the contribution due to the mean field to dominate over that due to the collisions. Therefore, the reduced in-medium σ_{np} leads to about the same or a slightly higher isospin transport. As the x parameter decreases to $x = -1$ and $x = -2$, however, the symmetry potential decreases and its density gradient can be even negative at low densities. In these cases, either the collisional contribution dominates or the mean-field contribution becomes negative. Therefore, the reduced in-medium np scattering cross-section $\sigma_{\rm np}$ leads to a weaker isospin transport compared with the case with the free-space NN cross-sections.

Based on an isospin- and momentum-dependent IBUU04 transport model with free-space experimental NN cross-sections, comparing the theoretical results with the experimental data has allowed us to extract a nuclear symmetry energy of $E_{\rm sym}(\rho) \approx 31.6(\rho/\rho_0)^{1.05}$. Including also medium-dependent NN cross-sections, which are important for isospin-dependent observables [116, 171], the isospin diffusion data leads to an even softer nuclear symmetry energy of $E_{\rm sym}(\rho) \approx 31.6(\rho/\rho_0)^{\gamma}$ with $\gamma \approx 0.69$ [121].

Since the slope parameter L of the nuclear symmetry energy gives an important constraint on the density dependence of the nuclear symmetry energy, in particular, it has been shown that the slope parameter L is related to the neutron skin thickness of heavy nuclei, it is interesting to see how the isospin diffusion data constrain the value of L. In Fig. 13, we show the results from the IBUU04 transport model with in-medium NN cross-sections, which are consistent with the mean-field potential obtained with the MDI interactions used in the model for the degree of the isospin diffusion $1 - R_i$ as a function of L. The shaded band in Fig.13 indicates the data from NSCL/MSU [117]. It is seen that the strength of isospin diffusion $1 - R_i$ decreases monotonically with decreasing value of x or increasing value of L. This is expected as the parameter L reflects the difference in the pressures on neutrons and protons. From comparison of the theoretical results with the data, we can clearly exclude the MDI interaction with $x = 1$ and $x = -2$ as they give either too large or too small a value for $1 - R_i$ compared to that of the data. The range of x or L values that give values of $1 - R_i$ falling within the band of experimental values could, in principle, be determined in our model by detailed calculations. Instead, we determine this schematically by using the results from the four x values. For the centroid value of L, it is obtained from the interception of the line connecting the theoretical results at $x = -1$ and 0 with the central value of $1 - R_i$ data in Fig. 13, i.e., $L = 88$ MeV. The upper limit of $L = 113$ MeV is estimated from the interception of the line connecting the upper error bars of the theoretical results at $x = -1$ and -2 with the lower limit of the data band of $1 - R_i$. Similarly, the lower limit of $L = 65$ MeV is estimated from the interception of the line connecting the lower error bars of the theoretical results at $x = 0$ and -1 with the upper limit of the data band of $1 - R_i$. This leads to an extracted value of $L = 88 \pm 25$ MeV as shown by the solid square with error bar in Fig. 13.

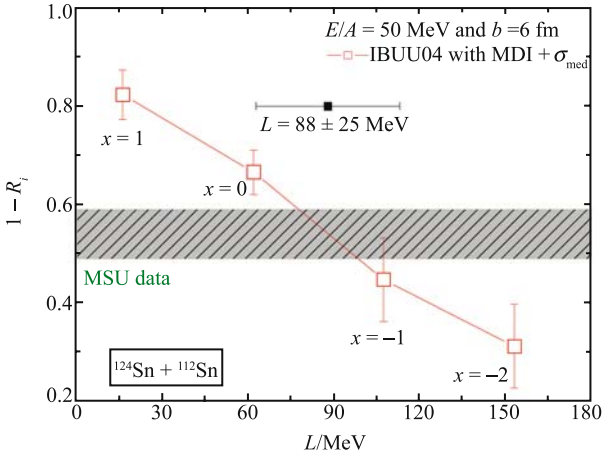

Fig.13 (*Color online*) Degree of the isospin diffusion $1 - R_i$ as a function of L using the MDI interaction with $x = -2$, -1, 0, and 1. The shaded band indicates the data from NSCL/MSU [117]. The solid square with error bar represents $L = 88 \pm 25$ MeV. Taken from Ref. [121].

5 Constraining the Skyrme effective interactions and the neutron skin thickness of nuclei using isospin diffusion data from heavy-ion collisions

Information on the density dependence of the nuclear symmetry energy can, in principle, also be obtained from the thickness of the neutron skin in heavy nuclei as the latter is strongly correlated with the slope parameter L of the nuclear symmetry energy at saturation density [10, 172−177]. Because of the large uncertainties in the measured neutron skin thickness of heavy nuclei, this has not been possible. Instead, studies have been carried out to use the extracted nuclear symmetry energy from the isospin diffusion data to constrain the neutron skin thickness of heavy nuclei [116, 119]. Using the Hartree-Fock approximation with parameters fitted to the phenomenological EOS that was used in the IBUU04 transport model to describe the isospin diffusion data from the NSCL/MSU, it was found that a neutron skin thickness of less than 0.15 fm [116, 119] for ^{208}Pb was incompatible with the isospin diffusion data.

In the following, we study more systematically the correlation between the density dependence of the nuclear symmetry energy and the thickness of the neutron skin in a number of nuclei within the framework of the Skyrme Hartree-Fock model. Using the extracted values of L from the isospin diffusion data in heavy-ion collisions, we obtain stringent constraints on the neutron skin thickness of the nuclei ^{208}Pb, ^{132}Sn, and ^{124}Sn. The extracted value of L also limits the allowed parameter sets for the Skyrme interaction.

5.1 Constraining the Skyrme effective interactions using isospin diffusion data

In the standard Skyrme Hartree-Fock model, the interaction is taken to have a zero-range, density- and momentum-dependent form [64, 178−181], i.e.,

$$\begin{aligned} V_{12}(\boldsymbol{R},\boldsymbol{r}) = {} & t_0(1+x_0P_\sigma)\delta(\boldsymbol{r}) \\ & + \frac{1}{6}t_3(1+x_3P_\sigma)\rho^\sigma(\boldsymbol{R})\delta(\boldsymbol{r}) \\ & + \frac{1}{2}t_1(1+x_1P_\sigma)[K^{'2}\delta(\boldsymbol{r})+\delta(\boldsymbol{r})K^2] \\ & + t_2(1+x_2P_\sigma)\boldsymbol{K}^{'}\cdot\delta(\boldsymbol{r})\boldsymbol{K} \\ & + \mathrm{i}W_0\boldsymbol{K}^{'}\cdot\delta(\boldsymbol{r})[(\sigma_{\boldsymbol{1}}+\sigma_{\boldsymbol{2}})\times\boldsymbol{K}] \end{aligned} \tag{16}$$

with $\boldsymbol{r}=\boldsymbol{r}_1-\boldsymbol{r}_2$ and $\boldsymbol{R}=(\boldsymbol{r}_1+\boldsymbol{r}_2)/2$. In the above, the relative momentum operators $\boldsymbol{K}=(\nabla_{\boldsymbol{1}}-\nabla_{\boldsymbol{2}})/2\mathrm{i}$ and $\boldsymbol{K}'=-(\nabla_{\boldsymbol{1}}-\nabla_{\boldsymbol{2}})/2\mathrm{i}$ act on the wave function on the right and left, respectively. The quantities P_σ and σ_i denote, respectively, the spin exchange operator and Pauli spin matrices. The σ, t_0-t_3, x_0-x_3, and W_0 are Skyrme interaction parameters that are chosen to fit the binding energies and charge radii of a large number of nuclei in the periodic table. For infinite nuclear matter, the symmetry energy from the Skyrme interaction can be expressed as [180, 181]

$$\begin{aligned} E_{\rm sym}(\rho) = {} & \frac{1}{3}\frac{\hbar^2}{2m}\left(\frac{3\pi^2}{2}\right)^{2/3}\rho^{2/3} \\ & - \frac{1}{8}t_0(2x_0+1)\rho - \frac{1}{48}t_3(2x_3+1)\rho^{\sigma+1} \\ & + \frac{1}{24}\left(\frac{3\pi^2}{2}\right)^{2/3}\left[-3t_1x_1+(4+5x_2)\,t_2\right]\rho^{5/3} \end{aligned} \tag{17}$$

The coefficient of the δ^4 term in Eq. (1) can also be obtained analytically and has been shown to be very small over a large range of nuclear density ($\leqslant 0.80$ fm^{-3}) and isospin asymmetry. The parabolic law of Eq. (1) without the δ^4 and higher-order terms in δ is thus justified [180].

Figure 14 displays the density dependence of $E_{\rm sym}(\rho)$ for 21 sets of Skyrme interaction parameters, i.e., SKM, SKM^*, $RATP$, SI, SII, $SIII$, SIV, SV, SVI, E, E_σ, G_σ, R_σ, Z, Z_σ, Z^*_σ, T, $T3$, SkX, $SkXce$, and $SkXm$. The values of the parameters in these Skyrme interactions can be found in Refs. [64, 178, 179]. For comparison, we also show in Fig. 14 results from the phenomenological MDI interactions with $x=-1$ (*open squares*) and 0 (*solid squares*). As we have discussed above, from comparing the isospin diffusion data from NSCL/MSU using the IBUU04 with in-medium NN cross-sections, these interactions are recently shown to give, respectively, the upper and lower bounds for the stiffness of the symmetry energy [116]. It is seen from Fig. 14 that the density dependence of the symmetry energy varies drastically among different interactions. Although the values of $E_{\rm sym}(\rho_0)$ are all in the range of $26-35$ MeV, the values of L and $K_{\rm sym}$ are in the range of $-50-100$ MeV and $-700-50$ MeV, respectively.

The extracted value of $L=88\pm25$ MeV gives a rather stringent constraint on the density dependence of the nuclear symmetry energy and thus puts strong constraints on the nuclear effective interactions as well. For the Skyrme effective interactions shown in Fig. 14, for instance, all of those lie beyond $x=0$ and $x=-1$ in the sub-saturation region are not consistent with the extracted value of L. Actually, we note that only 4 sets of Skyrme interactions, i.e., SIV, SV, G_σ, and R_σ, in the 21 sets of Skyrme interactions considered here have nuclear symmetry energies that are consistent with the extracted L value.

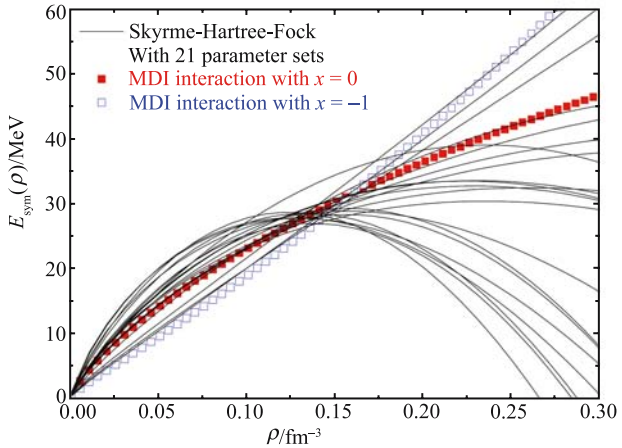

Fig.14 (*Color online*) Density dependence of the nuclear symmetry energy $E_{\rm sym}(\rho)$ for 21 sets of Skyrme interaction parameters. The results from the MDI interaction with $x = -1$ (*open squares*) and 0 (*solid squares*) are also shown. Taken from Ref. [121].

5.2 Constraining the neutron skin thickness of nuclei using isospin diffusion data

The neutron skin thickness S of a nucleus is defined as the difference between the root-mean-square radii $\sqrt{\langle r_{\rm n}\rangle}$ of neutrons and $\sqrt{\langle r_{\rm p}\rangle}$ of protons, i.e.,

$$S = \sqrt{\langle r_{\rm n}^2\rangle} - \sqrt{\langle r_{\rm p}^2\rangle} \tag{18}$$

It has been known that S is sensitive to the density dependence of the nuclear symmetry energy, particularly the slope parameter L at the normal nuclear matter density [10, 172−177]. Using the above 21 sets of Skyrme interaction parameters, we have evaluated the neutron skin thickness of several nuclei. In Figs. 15(a), (b) and (c), we show, respectively, the correlations between the neutron skin thickness of ^{208}Pb with L, $K_{\rm sym}$, and $E_{\rm sym}(\rho_0)$. It is seen from Fig.15(a) that there exists an approximate linear correlation between S and L. The correlations of S with $K_{\rm sym}$ and $E_{\rm sym}(\rho_0)$ are less strong and even exhibit some irregular behavior. The solid line in Fig. 15(a) is a linear fit to the correlation between S and L and is given by the following expression:

$$S(^{208}{\rm Pb}) = (0.1066 \pm 0.0019) + (0.001\,33 \pm 3.76 \times 10^{-5}) \times L \tag{19}$$

or

$$L = (-78.5 \pm 3.2) + (740.4 \pm 20.9) \times S(^{208}{\rm Pb}) \tag{20}$$

where the units of L and S are MeV and fm, respectively. Therefore, if the value for either $S(^{208}{\rm Pb})$ or L is known, the value for the other can be determined.

It is of interest to see if there are also correlations between the neutron skin thickness of other neutron-rich nuclei and the nuclear symmetry energy. Figure 16 shows the same correlations as in Fig. 16 but for the neutron-rich nuclei ^{132}Sn, ^{124}Sn, and ^{48}Ca. For the heavy ^{132}Sn and ^{124}Sn, we obtain a similar conclusion as for ^{208}Pb, namely, S exhibits an approximate linear correlation with L but weaker correlations with $K_{\rm sym}$ and $E_{\rm sym}(\rho_0)$. For the lighter ^{48}Ca, on the other hand, all the correlations become weaker than those of heavier nuclei. Therefore, the neutron skin thickness of heavy nuclei is better correlated with the density dependence of the nuclear symmetry energy. As in Eqs. (19) and (20), a linear fit to the correlation between S and L can also be obtained for ^{132}Sn and ^{124}Sn, and the corresponding expressions are

$$S(^{132}{\rm Sn}) = (0.1694 \pm 0.0025) + (0.0014 \pm 5.12 \times 10^{-5}) \times L \tag{21}$$

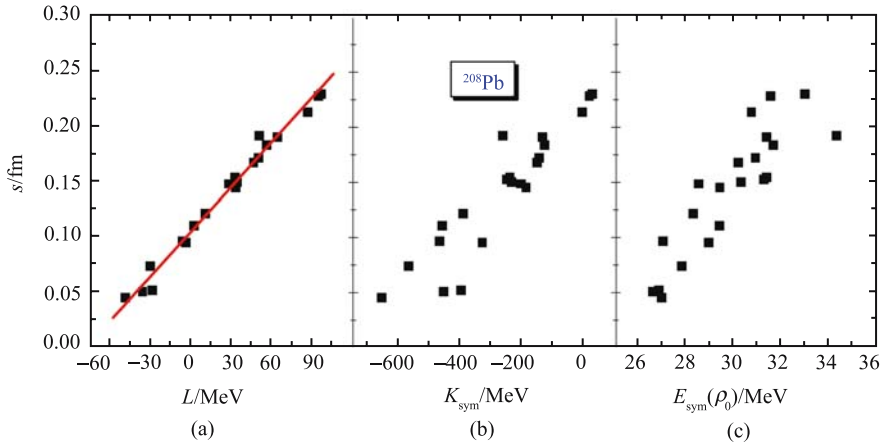

Fig.15 (*Color online*) Neutron skin thickness S of ^{208}Pb as a function of **(a)** L, **(b)** $K_{\rm sym}$, and **(c)** $E_{\rm sym}(\rho_0)$ for 21 sets of Skyrme interaction parameters. The line in panel (a) represents a linear fit. Taken from Ref. [121].

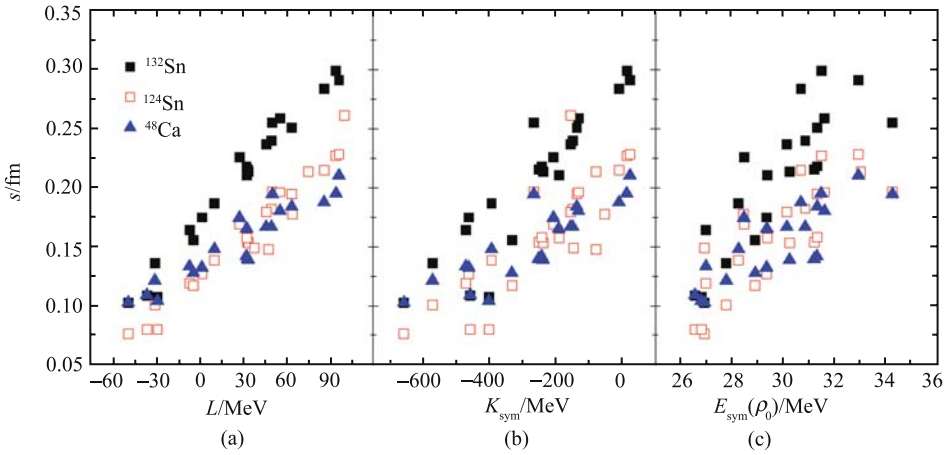

Fig.16 (*Color online*) Same as Fig. 2 but for nuclei ^{132}Sn (*solid squares*), ^{124}Sn (*open squares*) and ^{48}Ca (*triangles*). Taken from Ref. [121].

$$L=(-117.1\pm5.4)+(695.1\pm25.3)\times S(^{132}\mathrm{Sn}) \tag{22}$$

and

$$S(^{124}\mathrm{Sn})=(0.1255\pm0.0020)+(0.0011\pm4.05\times10^{-5})\times L \tag{23}$$

$$L=(-110.1\pm5.2)+(882.6\pm32.3)\times S(^{124}\mathrm{Sn}) \tag{24}$$

Similar linear relations between S and L are also expected for other heavy nuclei. This is not surprising as detailed discussions in Refs. [10, 172−177] have shown that the thickness of the neutron skin in heavy nuclei is determined by the pressure difference between neutrons and protons, which is proportional to the parameter L.

Table 2 Linear correlation coefficients C_l of S with L, $K_{\rm sym}$ and $E_{\rm sym}(\rho_0)$ for ^{208}Pb, ^{132}Sn, ^{124}Sn, and ^{48}Ca from 21 sets of Skyrme interaction parameters. Taken from Ref. [121].

C_l/%	^{208}Pb	^{132}Sn	^{124}Sn	^{48}Ca
S-L	99.25	98.76	98.75	93.66
S-$K_{\rm sym}$	92.26	92.06	92.22	86.99
S-$E_{\rm sym}$	87.89	85.74	85.77	81.01

To give a quantitative estimate of the above discussed correlations, we define the following linear correlation coefficient C_l:

$$C_l=\sqrt{1-q/t} \tag{25}$$

where

$$q=\sum_{i=1}^{n}[y_i-(A+Bx_i)]^2 \tag{26}$$

$$t=\sum_{i=1}^{n}n(y_i-\overline{y}),\quad \overline{y}=\sum_{i=1}^{n}ny_i/n \tag{27}$$

In the above, A and B are the linear regression coefficients, (x_i, y_i) are the sample points, and n is the number of sample points. The linear correlation coefficient C_l measures the degree of linear correlation, and $C_l=1$ corresponds to an ideal linear correlation. Table 2 gives the linear correlation coefficient C_l for the correlation of S with L, $K_{\rm sym}$ and $E_{\rm sym}(\rho_0)$ for ^{208}Pb, ^{132}Sn, ^{124}Sn, and ^{48}Ca shown in Figs. 15 and 16 for different Skyrme interactions. It is seen that these correlations become weaker with decreasing nucleus mass, and a strong linear correlation only exists between the S and L for the heavier nuclei ^{208}Pb, ^{132}Sn, and ^{124}Sn. Therefore, the neutron skin thickness of these nuclei can be extracted once the slope parameter L of the nuclear symmetry energy at saturation density is known.

The extracted L value from isospin diffusion data allows us to determine from Eqs. (19), (21), and (23), respectively, a neutron skin thickness of 0.22 ± 0.04 fm for ^{208}Pb, 0.29 ± 0.04 fm for ^{132}Sn, and 0.22 ± 0.04 fm for ^{124}Sn. Experimentally, great efforts were devoted to measure the thickness of the neutron skin in heavy nuclei [182, 183], and a recent review can be found in Ref. [184]. The data for the neutron skin thickness of ^{208}Pb indicate a large uncertainty, i.e., $0.1-0.28$ fm. Our results for the neutron skin thickness of ^{208}Pb are thus consistent with the present data but give a much stronger constraint. A large uncertainty is also found experimentally in the neutron skin thickness of ^{124}Sn, i.e., its value varies from 0.1 fm to 0.3 fm depending on the experimental method. The proposed experiment of parity-violating electron scattering from ^{208}Pb at the Jefferson Laboratory is expected to give another independent and more accurate measurement of its neutron skin thickness (within 0.05 fm), thus providing improved constraints on the density dependence of the nuclear symmetry

energy [185, 186].

Recently, an accurately calibrated relativistic parametrization based on the relativistic mean-field theory has been introduced to study the neutron skin thickness of finite nuclei [122]. This parametrization can describe simultaneously the ground state properties of finite nuclei and their monopole and dipole resonances. Using this parametrization, the authors predicted a neutron skin thickness of 0.21 fm in ^{208}Pb, 0.27 fm in ^{132}Sn, and 0.19 fm in ^{124}Sn [122, 169]. These predictions are in surprisingly good agreement with our results constrained by the isospin diffusion data in heavy-ion collisions.

In addition, the neutron skin thickness of the nucleus ^{90}Zr has recently been determined to be 0.07 ± 0.04 fm from the model-independent spin-dipole sum rule value measured from the charge-exchange spin-dipole excitations [187]. This value is reproduced by the symmetry energy with $L = 88 \pm 25$ MeV extracted from the isospin diffusion data in heavy-ion collisions, which predicts a neutron skin thickness of 0.088 ± 0.04 fm for ^{90}Zr.

6 Probing the high density behavior of the nuclear symmetry energy in heavy-ion reactions induced by high energy radioactive beams

Although significant progress has been made in the determination of the density dependence of the nuclear symmetry energy at sub-normal densities, the high density behavior of the nuclear symmetry energy is still poorly known. Fortunately, heavy-ion reactions, especially those induced by high-energy radioactive beams that are available at high-energy radioactive beam facilities, provide a unique opportunity to pin down the high density behavior of the symmetry energy. In this section, we illustrate via transport model simulations several experimental observables, which are sensitive to the high density behavior of the symmetry energy.

6.1 Isospin asymmetry of dense matter formed in high-energy heavy-ion reactions

To see the maximum baryon density and isospin asymmetry that can be achieved in central heavy-ion collisions induced by high energy radioactive beams in future radioactive beam facilities, we show in Fig. 17 the central baryon density [Fig.17(a)] and the average $(\mathrm{n/p})_{\rho \geqslant \rho_0}$ ratio [Fig.17(b)] of all regions with baryon densities higher than ρ_0 in the reaction of ^{132}Sn+^{124}Sn at a beam energy of 400 MeV/nucleon and an impact parameter of 1 fm. It is seen that the maximum baryon density is about 2 times normal nuclear matter density. Moreover, the compression is rather insensitive to the symmetry energy because the latter is relatively small compared to the EOS of symmetric matter around this density. The high density phase lasts for about 15 fm/c from 5 to 20 fm/c for this reaction. The isospin asymmetry of the high density region is, however, sensitive to the symmetry energy. The soft (e.g., $x = 1$) symmetry energy leads to a significantly higher value of $(\mathrm{n/p})_{\rho \geqslant \rho_0}$ than the stiff one (e.g., $x = -2$). This is consistent with the well-known isospin fractionation phenomenon that it is energetically more favorable to have a higher isospin asymmetry δ in the high density region for a softer symmetry energy functional $E_{\mathrm{sym}}(\rho)$ as a result of the $E_{\mathrm{sym}}(\rho)\delta^2$ term in the EOS of asymmetric nuclear matter. Since the symmetry energy changes from being soft to stiff when the parameter x varies from 1 to -2, the value of $(\mathrm{n/p})_{\rho \geqslant \rho_0}$ becomes lower in the supranormal density region as the parameter x changes from 1 to -2. Because of neutron-skins of the colliding nuclei, especially that of the projectile ^{132}Sn, the initial value of the quantity $(\mathrm{n/p})_{\rho \geqslant \rho_0}$, which is about 1.4, is less than the average $\mathrm{n/p}$ ratio of 1.56 of the reaction system. Also, in neutron-rich nuclei, the $\mathrm{n/p}$ ratio on the low-density surface is much higher than that in their interior. The dense matter region in heavy-ion collisions can thus become either neutron-richer or neutron-poorer with respect to the initial state depending on the symmetry energy functional $E_{\mathrm{sym}}(\rho)$ used.

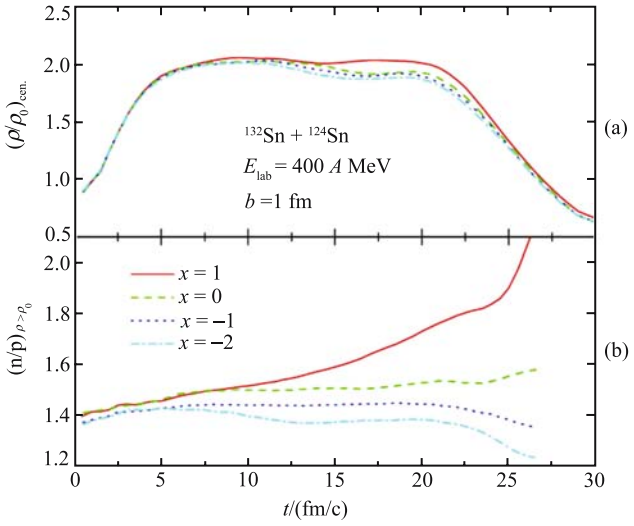

Fig.17 (*Color online*) Central baryon density **(a)** and isospin asymmetry **(b)** of high density region for the reaction of $^{132}\mathrm{Sn}+^{124}\mathrm{Sn}$ at a beam energy of 400 MeV/nucleon and an impact parameter of 1 fm. Taken from Ref. [102].

6.2 Isospin fractionation and n-p differential flow

The degree of isospin equilibration or translucency in heavy

ion collisions can be measured by the rapidity distribution of nucleon isospin asymmetry $\delta_{\rm free} \equiv (N_{\rm n} - N_{\rm p})/(N_{\rm n} + N_{\rm p})$, where $N_{\rm n}$ and $N_{\rm p}$ are multiplicities of free neutrons and protons, respectively [97, 98]. Although it might be difficult to directly measure $\delta_{\rm free}$ because it requires the detection of neutrons, similar information can be extracted from ratios of light clusters, such as, $t/^3$He, as demonstrated recently within a coalescence model [92, 93, 96]. Shown in Fig. 18 are rapidity distributions of $\delta_{\rm free}$ with [Fig.18(a)] and without [Fig.18(b)] the Coulomb potential. It is interesting to see that the $\delta_{\rm free}$ at midrapidity is particularly sensitive to the symetry energy. As the parameter x increases from -2 to 1 the $\delta_{\rm free}$ at midrapidity decreases by about a factor of 2. Moreover, the forward-backward asymmetric rapidity distributions of $\delta_{\rm free}$ with all four x parameters indicates the apparent nuclear translucency during the reaction [103].

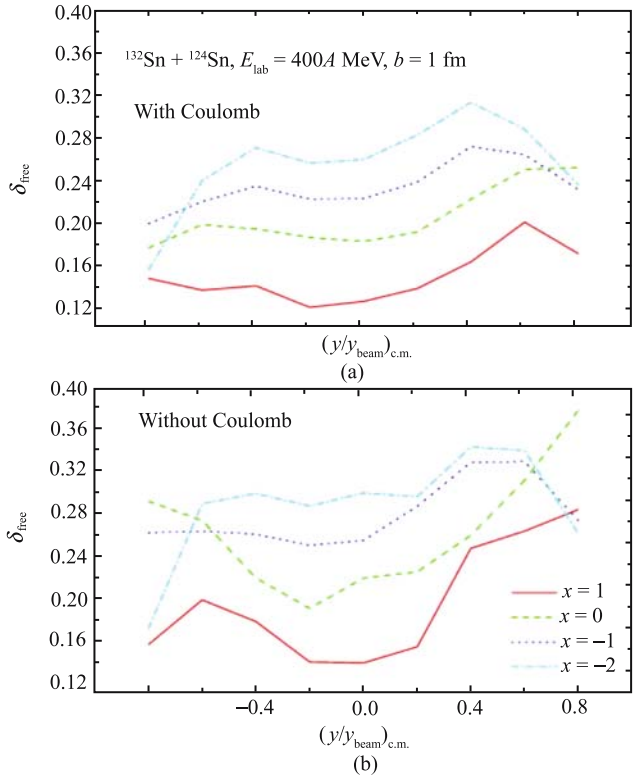

Fig.18 (*Color online*) Isospin asymmetry of free nucleons with and without the Coulomb force for different symmetry energies. Taken from Ref. [103].

Another observable that is sensitive to the high density behavior of the symmetry energy is the neutron-proton differential flow first introduced in Ref. [86]:

$$F^x_{\rm n-p}(y) \equiv \sum_{i=1}^{N(y)} (p^x_i w_i)/N(y) \tag{28}$$

where $w_i = 1(-1)$ for neutrons (protons) and $N(y)$ is the total number of free nucleons at rapidity y. Since the differential flow depends on the symmetry potential through the latter's effects on the isospin fractionation and the collective flow, it has the advantage of maximizing the effects of the symmetry potential while minimizing those of the isoscalar potential. Shown in Fig. 19 is the n-p differential flow for the reaction of ^{132}Sn+^{124}Sn at a beam energy of 400 MeV/nucleon and an impact parameter of 5 fm. Effects of the symmetry energy are clearly revealed by changing the parameter x.

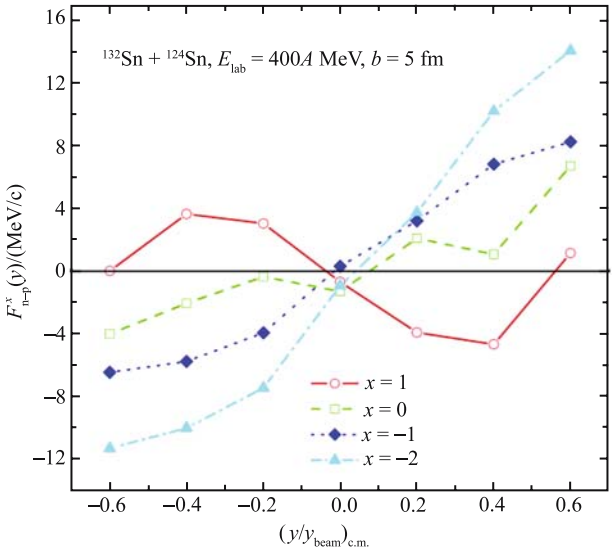

Fig.19 (*Color online*) Neutron-proton differential flow for different symmetry energies. Taken from Ref. [112].

6.3 Pion yields and π^-/π^+ ratio

At a beam energy of about 400 MeV/nucleon, pion production becomes non-negligible and may also carry interesting information about the EOS of dense neutron-rich matter [102, 188]. In Fig. 20, we show the π^- and π^+ yields as functions of the x parameter in the MDI interaction. It is seen that when the x parameter is changed from -2 to 1, the π^- multiplicity increases by about 20%, although the π^+ multiplicity remains about the same. The π^- multiplicity is thus more sensitive to the symmetry energy than that of π^+. Also, the multiplicity of π^- is about 2 to 3 times that of π^+. This is because π^- mesons are mostly produced from neutron-neutron collisions, which are more frequent in collisions of neutron-rich nuclei. Since the high density region is more neutron rich for the softer symmetry energy as a result of isospin fractionation [102], the π^- multiplicity is thus more sensitive to the isospin asymmetry of the reaction system and the symmetry energy. However, it is well known that the pion yield is also sensitive to the symmetric part of the nuclear EOS, and it is thus hard to extract reliable information about the symmetry energy from the π^- yield alone. The π^-/π^+ ratio is, on the other hand, a

better probe as this ratio is sensitive only to the difference in the chemical potentials for neutrons and protons [189, 190]. As well demonstrated in Fig. 21, the π^-/π^+ ratio is quite sensitive to the symmetry energy, especially at low transverse momenta, and can be used to probe the high density behavior of nuclear symmetry energy $E_{\rm sym}(\rho)$.

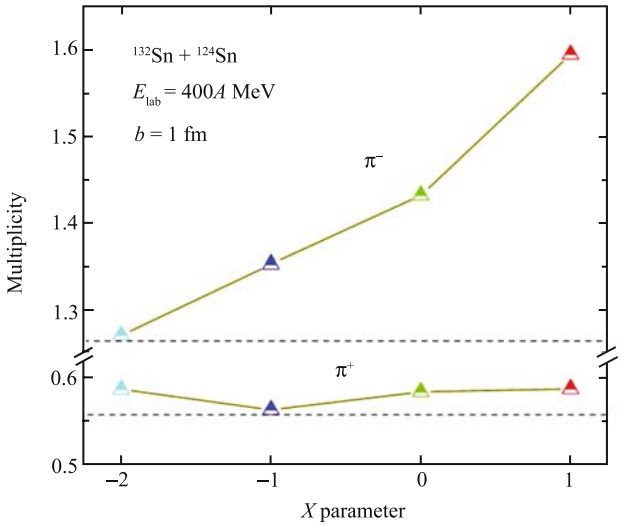

Fig.20 (*Color online*) The π^- and π^+ yields as functions of the x parameter. Taken from Ref. [102].

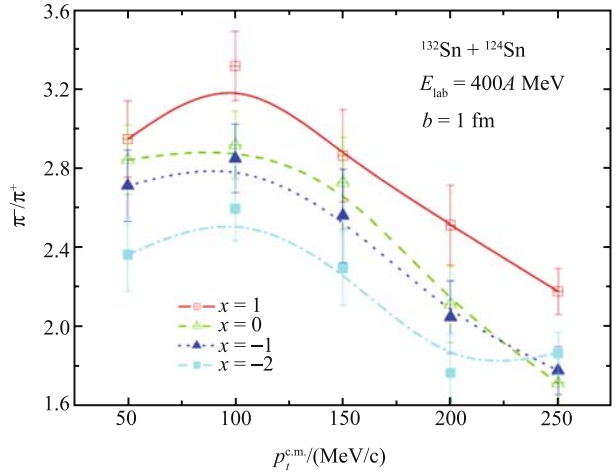

Fig.21 (*Color online*) The π^-/π^+ ratio as a function of transverse momentum. Taken from Ref. [102].

6.4 Double n/p and π^-/π^+ ratio

Because of the fact that the symmetry potentials have opposite signs for neutrons and protons and are also generally smaller compared to the isoscalar potential at the same density, most observables proposed so far for studying the density dependence of the nuclear symmetry energy employ differences or ratios of isospin multiplets of baryons, mirror nuclei and mesons, such as, the neutron/proton ratio of emitted nucleons [72], neutron-proton differential flow [86], neutron-proton correlation function [90, 91], $t/^3$He [92, 93, 104], π^-/π^+ [88, 89, 102, 108, 109], Σ^-/Σ^+ [105] and K^0/K^+ ratios [110, 111], etc. Among these observables, the ratio of emitted neutrons to protons has probably the highest sensitivity to the symmetry energy as the symmetry potential acts directly on nucleons and emitted nucleons are also rather abundant in typical heavy-ion reactions. However, it is very challenging to measure some of these observables, especially those involving neutrons. The measurement of neutrons, particularly the low energy ones, always suffers from low detection efficiencies even for the most advanced neutron detectors. Therefore, observables involving neutrons normally have large systematic errors. Moreover, for essentially all of these observables, the Coulomb force on charged particles plays an important role and sometimes competes strongly with the symmetry potential. One has to disentangle carefully the effects of the symmetry potential from those due to the Coulomb potential. It is thus very desirable to find experimental observables that can reduce the influence of both the Coulomb force and the systematic errors associated with neutrons. A possible candidate for such an observable is the double ratios of emitted neutrons and protons taken from two reaction systems using four isotopes of the same element, namely, the neutron/proton ratio in the neutron-rich system over that in the more symmetric system, as recently proposed by Lynch *et al.* [191, 192]. They have actually demonstrated the feasibility of measuring the double neutron/proton ratios in central reactions of ^{124}Sn+^{124}Sn and ^{112}Sn+^{112}Sn at a beam energy of 50 MeV/nucleon at the National Superconducting Cyclotron Laboratory [191, 192].

Both the double neutron/proton ratio and the double π^-/π^+ ratio in ^{132}Sn+^{124}Sn and ^{112}Sn+^{112}Sn reactions at 400 MeV/nucleon have been studied in the IBUU model in order to demonstrate the effect of symmetry energy at high density. It was found that these ratios have about the same sensitivity to the density dependence of symmetry energy as the corresponding single ratio in the respective neutron-rich system involved. Given the advantages of measuring the double ratios over the single ones, the study of double ratios will be more useful for further constraining the symmetry energy of neutron-rich matter. Furthermore, the systematic errors associated with transport model calculations are mostly related to the uncertainties in the in-medium NN cross-sections, techniques of treating collisions, sizes of the lattices in calculating the phase space distributions, and techniques in handling the Pauli blocking, etc. Since the double ratio is a relative observable from two similar reaction systems, these systematic

errors are expected to be reduced.

In Fig. 22, we show the double neutron/proton ratios from the reactions of ^{132}Sn+^{124}Sn and ^{112}Sn+^{112}Sn at a beam energy of 400 MeV/nucleon and an impact parameter of 1 fm [Fig.22(a)] and 5 fm [Fig.22(b)] predicted by the IBUU model using the MDI interaction with $x = 0$ and $x = -1$, which are consistent with the symmetry energy used for sub-saturation densities. At both impact parameters, effects of the symmetry energy are about $5\% - 10\%$ changing from the case with $x = 0$ to $x = -1$. One notices here that the low energy nucleons have the largest sensitivity to the variation of the symmetry energy for such high energy heavy-ion collisions. In fact, the neutron/proton ratio of midrapidity nucleons that have gone through the high density phase of the reaction are known to be most sensitive to the symmetry energy [103]. Compared to the results at the beam energy of 50 MeV/nucleon [193], it is interesting to see a clear turnover in the dependence of the double neutron/proton ratio on the x parameter, namely the double ratio is lower at 50 MeV/nucleon but higher at 400 MeV/nucleon with $x = -1$ than that with $x = 0$. The maximum density reached at the beam energy of 50 and 400 MeV/nucleon is about $1.2\rho_0$ and $2\rho_0$ [193], respectively. The turnover clearly indicates that the double neutron/proton ratio reflects closely the density dependence of the symmetry energy as shown in Fig. 2. This observation also indicates that systematic studies of the double neutron/proton ratio over a broad beam energy range will be important for mapping out the density dependence of the symmetry energy.

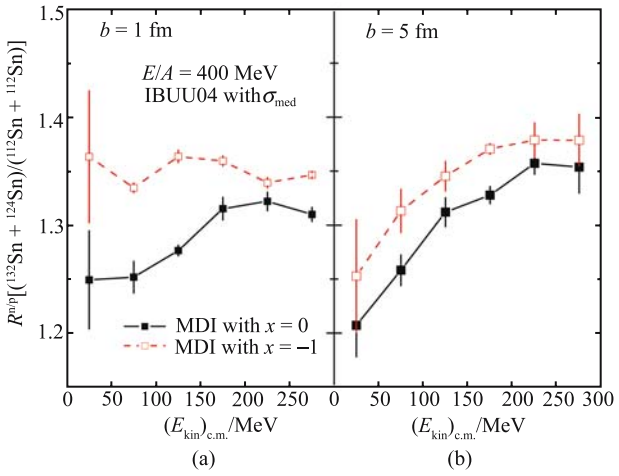

Fig.22 (*Color online*) The double neutron/proton ratio of free nucleons in the reaction of ^{132}Sn +^{124}Sn and ^{112} Sn+^{112}Sn at 400 MeV/nucleon and an impact parameter of 1 fm **(a)** and 5 fm **(b)**, respectively. Taken from Ref. [193].

As shown before from both the total yields and the momentum spectra, the π^-/π^+ ratio is a promising probe of the symmetry energy at high densities [88, 89, 102, 105, 108]. In Fig. 23, we show again the kinetic energy distribution of the single π^-/π^+ ratio for the reactions of ^{132}Sn+^{124}Sn and ^{112}Sn+^{112}Sn at a beam energy of 400 MeV/nucleon and an impact parameter of $b = 1$ fm with the stiff ($x = -1$) or soft ($x = 0$) symmetry energy, obtained with 12 000 IBUU events for each reaction. It is seen that the overall magnitude of π^-/π^+ ratio is larger for the neutron-rich system ^{132}Sn+^{124}Sn than for the neutron-deficient system ^{112}Sn+^{112}Sn as expected. Also, the soft symmetry energy ($x = 0$) leads to a larger single π^-/π^+ ratio than the stiff one ($x = -1$). This is mainly because the high density region where most pions are produced are more neutron-rich with the softer symmetry energy as a result of the isospin fractionation [88, 89, 102]. Furthermore, the single π^-/π^+ ratio is more sensitive to the symmetry energy in the reaction ^{132}Sn+^{124}Sn than in the reaction ^{112}Sn+^{112}Sn as a result of the larger isospin asymmetry in the more neutron-rich system.

Figure 23 shows that the single π^-/π^+ ratio exhibits a peak at a pion kinetic energy of about 45 MeV in all cases considered here. The origin of this peak can be understood from the single π^-/π^+ ratios in both reactions from turning off the Coulomb potentials for all charged particles. As an example, shown in Fig.23 with the dash-dotted line is the single π^-/π^+ ratio obtained by turning off the Coulomb potentials in the ^{132}Sn+^{124}Sn reaction. It is seen that the single π^-/π^+ ratio now becomes approximately a constant of about 2.4. This value agrees with the predicted value of

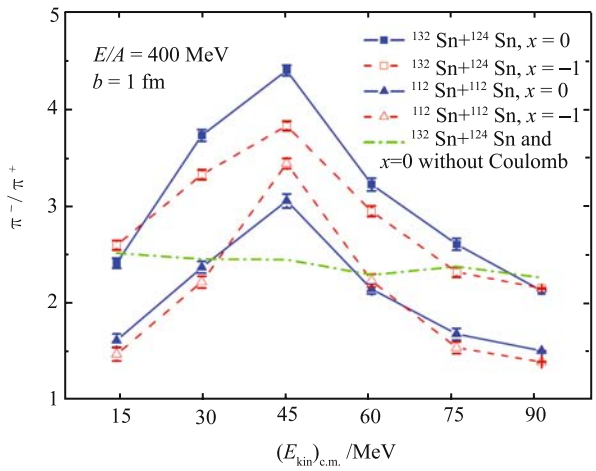

Fig.23 (*Color online*) Kinetic energy distribution of the single π^-/π^+ ratio for ^{132}Sn+^{124}Sn and ^{112}Sn+^{112}Sn at a beam energy of 400 MeV/nucleon and an impact parameter of $b = 1$ fm with the stiff ($x = -1$) and soft ($x = 0$) symmetry energies. The dash-dotted line is the single π^-/π^+ ratio obtained by turning off the Coulomb potentials in the ^{132}Sn+^{124}Sn reaction. Taken from Ref. [194].

$(5N^2 + NZ)/(5Z^2 + NZ) \approx (N/Z)^2 \approx 2.43$, where N and Z are the total neutron and proton numbers in the participant region, from the Δ resonance model [195] for central ^{132}Sn+^{124}Sn collisions. This is not surprising as at 400 MeV/nucleon, pions are almost exclusively produced via the Δ resonances [196]. Comparison of calculated results with and without the Coulomb potentials thus indicates clearly that the peak observed in the single π^-/π^+ ratio is due to the Coulomb effects. Although the Coulomb potential distorts the spectra of pions, the effect of symmetry potential is still seen in the resulting π^-/π^+, particularly near its peak value where pions have relatively low kinetic energies. These pions are produced in the high density nucleonic matter (about $2\rho_0$) through the Δ resonances and experience many rescatterings with nucleons at both high and low densities as well as the Coulomb potential from protons at different densities. Since the soft ($x = 0$) and stiff ($x = -1$) symmetry energies have slight difference at low densities and the large difference appears at high densities (about $2\rho_0$) as shown in Fig. 2, the observed symmetry energy effects on the energy dependence of the π^-/π^+ ratio thus mainly reflect (though not completely) information on the high density behavior of the symmetry energy [109].

In order to reduce the systematic errors related to the symmetry energy effect on the π^-/π^+ ratio, it is more useful to study the double π^-/π^+ ratio in the reactions of ^{132}Sn+^{124}Sn and ^{112}Sn+^{112}Sn as for the double proton/neutron ratio. Figure 24 shows the double π^-/π^+ ratio for these two reactions. It is seen that the kinetic energy dependence of the double π^-/π^+ ratio is rather different for the stiff ($x = -1$) and soft ($x = 0$) symmetry energies. While the double π^-/π^+ ratio is quite flat for $x = 0$, it displays a concave structure for $x = -1$ around the Coulomb peak. These different behaviors can be understood from the corresponding single π^-/π^+ ratios in the two reactions shown in Fig. 23. It is reassuring to see that around the Coulomb peak the double π^-/π^+ ratio is still sensitive to the symmetry energy. Compared with the single π^-/π^+ ratio, the kinetic energy dependence of the double π^-/π^+ ratio becomes, however, weaker. This is because effects of the Coulomb potentials are reduced in the double π^-/π^+ ratio. We note that the double π^-/π^+ ratio displays an opposite symmetry energy dependence compared with the double n/p ratio for free nucleons shown in Fig. 22. This is understandable since the soft symmetry energy leads to a more neutron-rich dense matter in heavy-ion collisions induced by neutron-rich nuclei and thus a smaller n/p ratio for free nucleons due to the charge conservation. On the other hand, more π^-'s would be produced due to more neutron-neutron inelastic scatterings in the more neutron-rich matter.

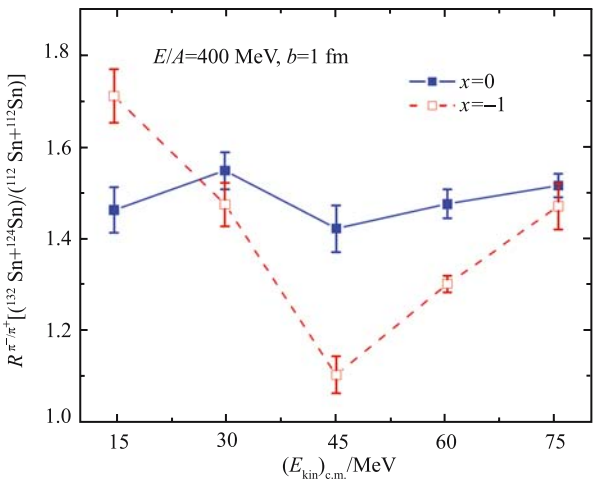

Fig.24 (*Color online*) Kinetic energy dependence of the double π^-/π^+ ratio of ^{132}Sn+^{124}Sn over ^{112}Sn+^{112}Sn at a beam energy of 400 MeV/nucleon and an impact parameter $b = 1$ fm with the stiff ($x = -1$) and soft ($x = 0$) symmetry energies. Taken from Ref. [194].

6.5 Double neutron-proton differential transverse flow

The neutron-proton differential transverse flow defined in Eq. (28) can be further expressed as [86, 88, 89, 102]

$$F^x_{\rm n-p}(y) \equiv \frac{1}{N(y)} \sum_{i=1}^{N(y)} p^x_i(y) w_i = \frac{N_{\rm n}(y)}{N(y)} \langle p^x_{\rm n}(y)\rangle - \frac{N_{\rm p}(y)}{N(y)} \langle p^x_{\rm p}(y)\rangle \quad (29)$$

where $N(y)$, $N_{\rm n}(y)$ and $N_{\rm p}(y)$ are the numbers of free nucleons, neutrons, and protons, respectively, at rapidity y; $p^x_i(y)$ is the transverse momentum of a free nucleon at rapidity y; $w_i = 1$ (-1) for neutrons (protons); and $\langle p^x_{\rm n}(y)\rangle$ and $\langle p^x_{\rm p}(y)\rangle$ are, respectively, the average transverse momenta of neutrons and protons at rapidity y. Eq. (29) shows that the neutron-proton differential transverse flow depends not only on the proton and neutron transverse momenta but also on their relative multiplicities, i.e., the isospin fractionation. This can be more clearly seen from the following two special cases. If neutrons and protons have the same average transverse momentum in the reaction plane but different multiplicities in each rapidity bin, i.e., $\langle p^x_{\rm n}(y)\rangle = \langle p^x_{\rm p}(y)\rangle = \langle p^x(y)\rangle$, and $N_{\rm n}(y) \neq N_{\rm p}(y)$, then Eq. (29) is reduced to

$$F^x_{\rm n-p}(y) = \frac{N_{\rm n}(y) - N_{\rm p}(y)}{N(y)} \langle p^x(y)\rangle = \delta(y) \cdot \langle p^x(y)\rangle \quad (30)$$

reflecting the effects of isospin fractionation. On the other hand, if neutrons and protons have the same multiplicity but different average transverse momenta, i.e., $N_{\rm n}(y) = N_{\rm p}(y)$ but $\langle p^x_{\rm n}(y)\rangle \neq \langle p^x_{\rm p}(y)\rangle$, then Eq. (29) is reduced to

$$F^x_{\rm n-p}(y) = \frac{1}{2}(\langle p^x_{\rm n}(y)\rangle - \langle p^x_{\rm p}(y)\rangle) \quad (31)$$

and reflects directly the difference between the neutron and proton transverse flows. Since a stiffer symmetry potential is expected to lead to a higher isospin fractionation and also a larger transverse flow for neutrons than for protons in heavy-ion collisions at higher energies, the neutron-proton differential flow is thus a measure of these two combined effects of the symmetry potentials on neutrons and protons [193, 194].

Shown in Fig. 25 are the rapidity distributions of the isospin asymmetry of free nucleons (upper panels), the difference of the average nucleon transverse flows (middle panels), and the neutron-proton differential transverse flow (lower panels) from the ^{132}Sn+^{124}Sn reaction at incident beam energies of 400 and 800 MeV/nucleon and an impact parameter of $b = 5$ fm with the two symmetry energies of $x = 0$ and $x = -1$. It can be seen that the stiffer symmetry energy ($x = -1$) leads to a larger isospin asymmetry of free nucleons (stronger isospin fractionation) (*upper panels*) than the softer symmetry energy ($x = 0$). As a result, the neutron-proton differential transverse flow from the stiff symmetry energy ($x = -1$) (*bottom panels*) is much larger than that from the soft symmetry energy ($x = 0$) compared to the difference between the average neutron and proton transverse flows obtained from the two symmetry energies (*middle panels*). Also, the negative (positive) values of the neutron and proton average transverse flow $F^x_{\rm n} - F^x_{\rm p}$ at forward (backward) rapidities as a result of the Coulomb potential effect on protons is reversed for the neutron-proton differential flow $F^x_{\rm n-p}(y)$ after taking into account the effect due to isospin fractionation.

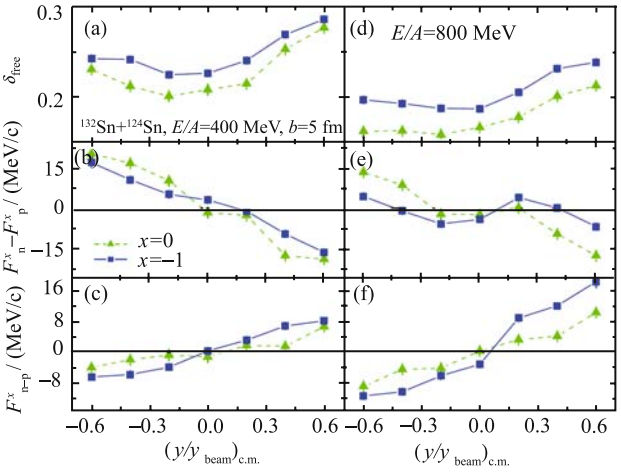

Fig.25 (*Color online*) Rapidity distributions of the isospin asymmetry of free nucleons (*upper panels*), the difference of the average nucleon transverse flows (middle panels) and the neutron-proton differential transverse flow (*lower panels*) from ^{132}Sn+^{124}Sn reaction at the incident beam energies of 400, 800 MeV/nucleon and $b = 5$ fm with two symmetry energies of $x = 0$ and $x = -1$. Taken from Ref. [197].

From panels (c) and (f) of Fig. 25, it is seen that the slope of the neutron-proton differential transverse flow around the mid-rapidity obtained from the same symmetry energy is larger for the higher incident beam energy. This is mainly because a denser nuclear matter is formed at higher incident beam energy, leading to a stronger symmetry potential and thus higher transverse momenta for neutrons compared to protons. Although the net effect of the symmetry potential on the neutron-proton differential transverse flow at 800 MeV/nucleon is not much larger than that at 400 MeV/nucleon, its magnitude is much larger and is thus easier to be measured experimentally.

The systematic errors in the neutron-proton differential flow can be reduced by studying its values in two similar reaction systems. Besides the ^{132}Sn+^{124}Sn reaction involving neutron-rich nuclei, one can consider another less neutron-rich reaction system ^{112}Sn+^{112}Sn. Figure 26 shows the rapidity distribution of the neutron-proton differential transverse flow in the semi-central reaction of ^{112}Sn+^{112}Sn at the same incident beam energies of 400 and 800 MeV/nucleon. In comparison with the ^{132}Sn+^{124}Sn reaction, the slope of the neutron-proton differential transverse flow around mid-rapidity and effects of the symmetry energy are much smaller due to the smaller isospin asymmetry in the reaction of ^{112}Sn+^{112}Sn.

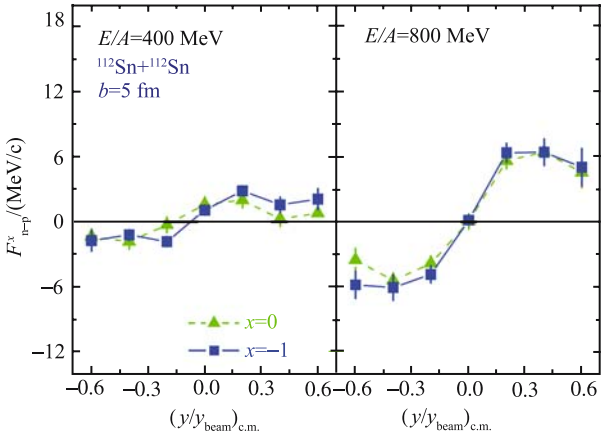

Fig.26 (*Color online*) Same as panels (c) and (f) of Fig. 25 but for the reaction system of ^{112}Sn+^{112}Sn. Taken from Ref. [197].

The double neutron-proton differential flow is defined as the difference of the neutron-proton differential flows in the two reaction systems of ^{132}Sn+^{124}Sn and ^{112}Sn+^{112}Sn. Figure 27 shows the rapidity distribution of the double neutron-proton differential transverse flow in the semi-central reactions of Sn+Sn isotopes. At both incident beam energies of 400 and 800 MeV/nucleon, the double neutron-proton differential transverse flow around mid-rapidity is essentially zero

for the soft symmetry energy of $x = 0$. It displays, however, a finite slope with respect to the rapidity for the stiffer symmetry energy of $x = -1$. Moreover, the double neutron-proton differential transverse flow at the higher incident energy exhibits a stronger symmetry energy effect as expected. Since the double neutron-proton differential transverse flow retains about the same symmetry energy effect as the ^{132}Sn+^{124}Sn reaction, it is less sensitive to the systematic uncertainties in experiments [167].

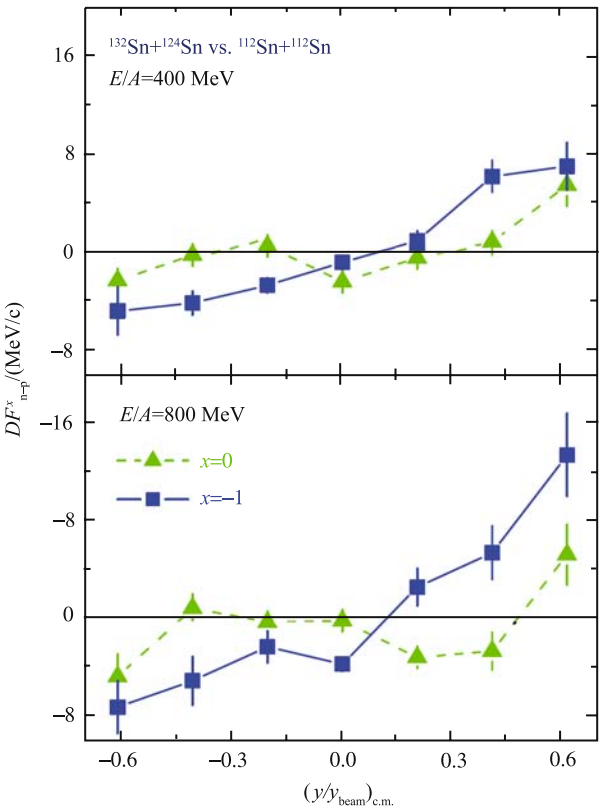

Fig.27 (*Color online*) Rapidity distribution of the double neutron-proton differential transverse flow in semi-central reactions of Sn+Sn isotopes at incident beam energies of 400 and 800 MeV/nucleon with two symmetry energies of $x = 0$ and $x = -1$. Taken from Ref. [197].

Also, the Coulomb effect, which competes strongly with the symmetry potentials, is less important in the double neutron-proton differential transverse flow than in the neutron-proton differential transverse flow. This can be seen in Fig. 28 which shows the neutron-proton differential transverse flow [Fig.28(a),(b)] and the double neutron-proton differential transverse flow [Fig.28(c)] in the semi-central reactions of Sn+Sn isotopes at the incident beam energy of 400 MeV/nucleon with the symmetry energy of $x = 0$ for the two cases of with and without the Coulomb potential. From the upper two panels of Fig. 28, one sees that the Coulomb effect reduces the strength of the neutron-proton differential transverse flow as it makes more protons unbound and to have large transverse momenta in the reaction-plane. The Coulomb effect is, however, largely reduced in the double neutron-proton differential transverse flow shown in the bottom panel of Fig. 28.

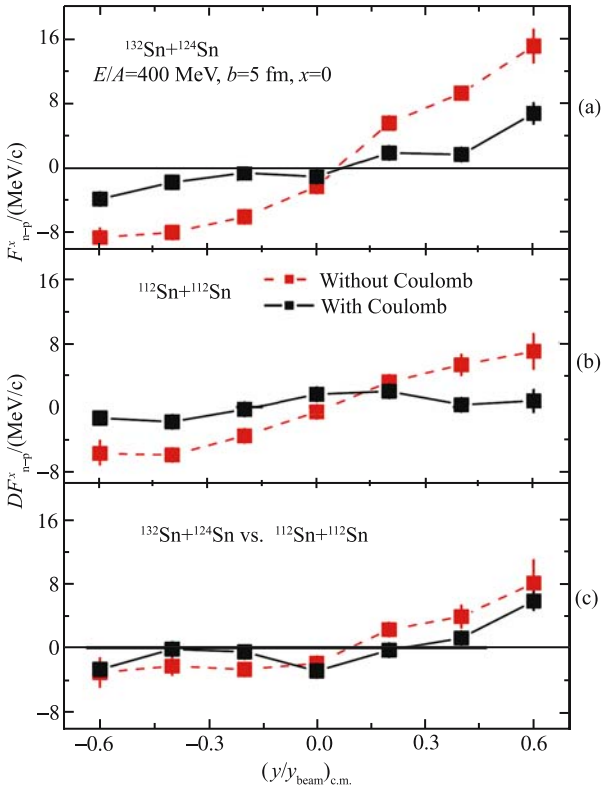

Fig.28 (*Color online*) Coulomb effects on the neutron-proton differential transverse flow **(a, b)** and the double neutron-proton differential transverse flow **(c)** in the semi-central reactions of Sn+Sn isotopes at the incident beam energy of 400 MeV/nucleon with the symmetry energy of $x = 0$. Taken from Ref. [197].

6.6 The n/p ratio of squeezed-out nucleons

It is well known that in noncentral heavy-ion collisions nucleons in the participant region is squeezed out of the reaction plane as a result of the large density gradient in this direction and the absence of spectator nucleons to block their emissions. These nucleons can thus carry direct information about the high density phase of the reaction and have been widely used in probing the EOS of dense matter, particularly that of the symmetric nuclear matter, see, e.g., Refs. [3, 114, 115, 198−200] for a review.

The possibility of using the squeezed out nucleons to study the high density behavior of the nuclear symmetry energy has been studied recently using the IBUU04 model [113]. Shown

in Fig. 29 are the azimuthal distributions of free nucleons in the midrapidity region ($|(y/y_{\rm beam})_{\rm c.m.}| < 0.5$) of the reaction ^{132}Sn+^{124}Sn at an incident beam energy of 400 MeV/nucleon and an impact parameter of $b = 5$ fm, predicted by the IBUU model using the MDI interactions with $x = 0$ and -1. A preferential emission of nucleons perpendicular to the reaction plane is clearly observed for both neutrons and protons. The sensitivity to the nuclear symmetry energy is mainly seen in the squeezed-out neutrons, which experience a stronger repulsive symmetry potential for a stiff ($x = -1$) than for a soft ($x = 0$) nuclear symmetry energy in the neutron-rich matter, in addition to the strong nuclear isoscalar potential. For protons, their azimuthal distributions is less sensitive to the stiffness of the nuclear symmetry energy. This is due to the additional repulsive Coulomb potential which works against the attractive symmetry potential experienced by protons in the neutron-rich matter. Although it is not easy to measure neutrons in experiments, both the transverse flow and squeeze-out of neutrons together with other charged particles were measured at both the BEVALAC [201] and SIS/GSI [202−204]. These experiments and the associated theoretical calculations, see, e.g., Refs. [205, 206], have, however, all focused on extracting information about the EOS of symmetric nuclear matter without paying much attention to the effects due to the nuclear symmetry energy.

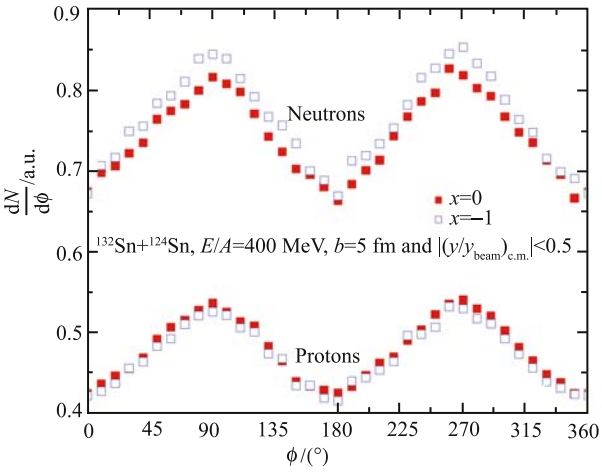

Fig.29 (*Color online*) Azimuthal distribution of midrapidity nucleonsemitted in the reaction of ^{132}Sn+^{124}Sn at an incident beam energy of 400 MeV/nucleon and an impact parameter of $b = 5$ fm. Taken from Ref. [113].

To reduce the effect due to uncertainties associated with the EOS of symmetric nuclear matter, it is useful to consider the ratio of squeezed-out neutrons to protons, particularly its transverse momentum dependence. As shown in Refs. [1, 72], the n/p ratio is determined mostly by the density dependence of the symmetry energy and almost not affected by the EOS of symmetric nuclear matter. In Fig. 30, we show the transverse momentum dependence of the neutron/proton (n/p) ratio of midrapidity nucleons emitted in the reaction of ^{132}Sn+^{124}Sn at the incident beam energy of 400 MeV/nucleon and impact parameter of $b = 5$ fm. For squeezed-out nucleons emitted in the direction perpendicular to the reaction plane, which are obtained by introducing an azimuthal angle cut of $80^\circ < \phi < 100^\circ$ and $260^\circ < \phi < 280^\circ$, the symmetry energy effect on the n/p ratio increases with the increasing transverse momentum p_t as shown in the lower window. The effect can be as large as 40% at a transverse momentum of 1 GeV/c. Since high p_t particles most likely come from the high density region in the early stage during heavy-ion collisions, they are thus more sensitive to the high density behavior of the symmetry energy. Without the cut on the azimuthal angle, the n/p ratio of free nucleons in the midrapidity region is much less sensitive to the symmetry energy in the whole range of transverse momentum as shown in the upper window. It is worth mentioning that the n/p ratio of free nucleons perpendicular to the beam direction in the CMS

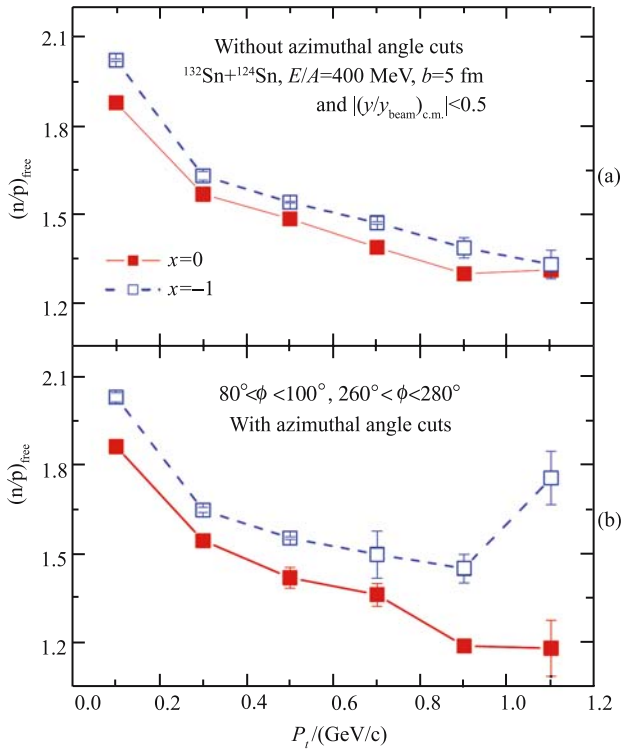

Fig.30 (*Color online*) Transverse momentum distribution of the ratio of midrapidity neutrons to protons emitted in the reaction of^{132}Sn+^{124}Sn at the incident beam energy of 400 MeV/nucleon and impact parameter of $b = 5$ fm, with **(b)** and without **(a)** an azimuthal angle cut of $80^\circ < \phi < 100^\circ$ and $260^\circ < \phi < 280^\circ$, which corresponds to squeezed-out nucleons emitted in the direction perpendicular to the reaction plane. Taken from Ref. [113].

frame in ^{124}Sn+^{124}Sn reactions at 50 MeV/nucleon was recently measured at the NSCL/MSU [192]. This measurement was useful for studying the density dependence of the symmetry energy at sub-normal densities. To investigate the symmetry energy at supra-normal densities, similar measurements that allow the construction of the reaction plane using a TPC (Time-Projection-Chamber) and simultaneous detection of neutrons together with charged particles at much higher energies are being planned [207]. The results reviewed here provide strong scientific motivations and support for such experimental efforts. Compared to other potential probes, the n/p ratio of squeezed-out nucleons is complementary but carries more direct information about the symmetry energy at high densities. The sensitivity to the high density behavior of the nuclear symmetry energy observed in the n/p ratio of squeeze-out nucleons is probably the highest found so far among all observables studied within the same transport model.

6.7 K^0/K^+ and Σ^-/Σ^+ ratios

Since the proposal of Aichelin and Ko that the kaon yield in heavy-ion collisions at energies that are below the threshold for kaon production in a nucleon-nucleon collision in free space may be a sensitive probe of the EOS of nuclear matter at high densities [208], a lot of works have been done both theoretically and experimentally on this problem [199, 209−213]. Since the kaon is an iso-doublet meson with the quark content of $d\bar{s}$ for K^0 and $u\bar{s}$ for K^+, the K^0/K^+ ratio provides a potentially good probe of the nuclear symmetry energy as the n/p and π^-/π^+ ratios, especially its high density behavior as kaons are produced mainly from the high density region during the early stage of the reaction and suffer negligible absorption effects.

Using the UrQMD model (Version 1.3), Li *et al.* have investigated the symmetry energy effects on the K^0/K^+ ratio by studying K^0 and K^+ production from the central ^{132}Sn+^{132}Sn collisions at a beam energy $1.5A$ GeV with two different forms of the symmetry energy, namely, the F15 and Fa3, and the results are shown in Fig. 31 [214]. Since the beam energy is close to the kaon production threshold, which is about 1.58 GeV for nucleon-nucleon collisions in free space, the K^0/K^+ ratio displays only a small symmetry energy effect. With decreasing beam energy, the symmetry energy effect becomes larger. For example, the kaon yields from the reaction ^{208}Pb+^{208}Pb at $E_b = 0.8$ A GeV and $b = 7 - 9$ fm, the K^0/K^+ ratio for the stiff F15 is about 1.25, whereas it is about 1.4 for the soft Fa3. We note that nuclear in-medium effects on kaon production are neglected in the UrQMD model simulations.

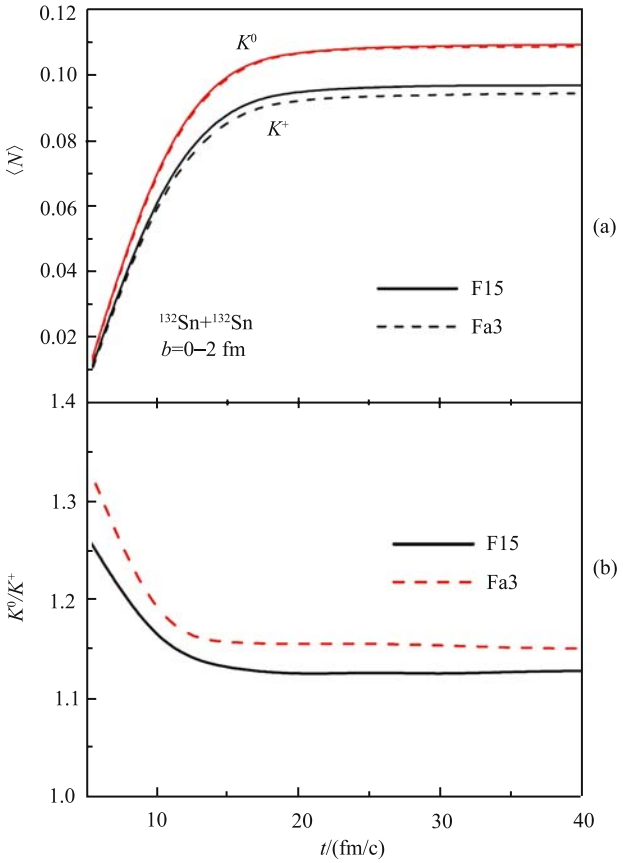

Fig.31 (*Color online*) **(a)** Time evolution of the K^0 and K^+ abundances for central ^{132}Sn $+^{132}$ Sn collisions at a beam energy $1.5A$ GeV and with the symmetry potentials F15 and Fa3. **(b)** the corresponding time evolution of the K^0/K^+ ratios. Taken from Ref. [214].

The above results were confirmed by Ferini et al. using a relativistic hadronic transport model of Boltzmann-Uehling-Uhlenbeck type (RBUU) with different forms of the symmetry energies in central ($b = 0$ fm impact parameter) Au+Au collisions [110, 111]. Their results, shown in Fig. 32, indicate that at beam energies below and around the kinematical threshold of kaon production, the K^0/K^+ inclusive yield ratio is more sensitive to the symmetry energy than the π^-/π^+, and subthreshold kaon production thus could provide a promising tool to extract information on the density dependence of the nuclear symmetry energy.

Experimentally, the FOPI collaboration has reported recently the results on K^+ and K^0 meson production in $^{96}_{44}$Ru + $^{96}_{44}$Ru and $^{96}_{40}$Zr + $^{96}_{40}$Zr collisions at a beam kinetic energy of 1.528 A GeV, measured with the FOPI detector at GSI-Darmstadt [215]. The measured double ratio $(K^+/K^0)_{\rm Ru}/(K^+/K^0)_{\rm Zr}$ is compared in Fig.33 to the predictions of a thermal model and the RBUU transport model using two different collision scenarios and un-

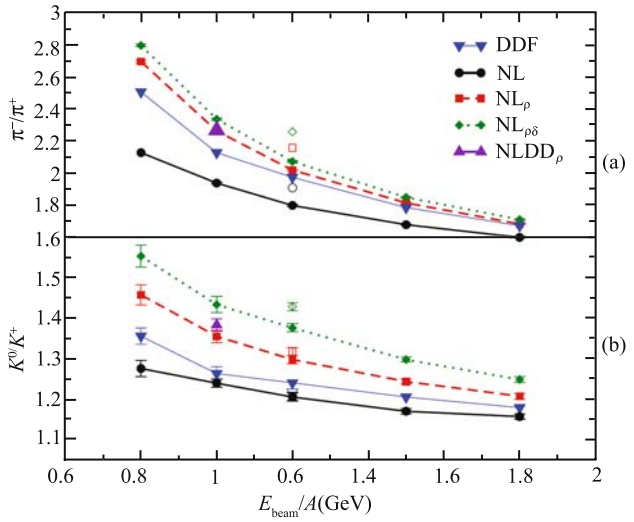

Fig.32 (*Color online*) π^-/π^+ **(a)** and K^+/K^0 **(b)** ratios as a function of the incident energy for central ($b = 0$ fm impact parameter) Au+Au collisions with the RBUU model. In addition, for $E_{\rm beam} = 1$ A GeV, NL$_\rho$ results with a density dependent ρ-coupling (*triangles*) are also presented. The *open* symbols at 1.2 A GeV show the corresponding results for a ^{132}Sn $+^{124}$ Sn collision, more neutron rich. Note the different scale for the π^-/π^+ ratios. Taken from Ref. [110, 111].

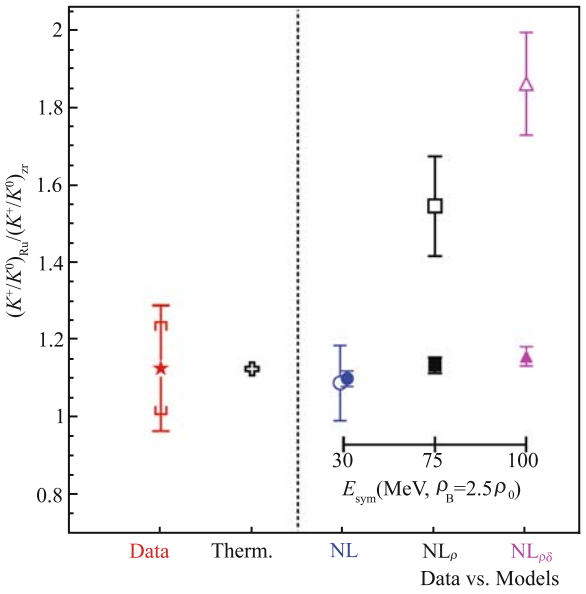

Fig.33 (*Color online*) Experimental ratio $(K^+/K^0)_{\rm Ru}/(K^+/K^0)_{\rm Zr}$ (*star*) and theoretical predictions of the thermal model (*cross*) and the transport model with 3 different assumptions on the symmetry energy: NL (*circles*), NL$_\rho$ (*squares*) and NL$_{\rho\delta}$ (*triangles*). The INM and HIC calculations are represented by open and full symbols, respectively (see text for more details). The statistic and systematic errors are represented by vertical bars and brackets, respectively. Taken from Ref. [215].

der different assumptions on the stiffness of the symmetry energy. From Fig.33, one can see a good agreement with the thermal model prediction and the assumption of a soft symmetry energy for infinite nuclear matter while more realistic transport simulations of the collisions show a similar agreement with the data but exhibit a reduced sensitivity to the symmetry term. We note that in the present RBUU calculations, the isospin dependence of the K^+- and K^0-nucleon potentials in the asymmetric nuclear medium has been neglected. Recently, Mishra *et al.* studied the isospin dependent kaon and antikaon optical potentials in dense hadronic matter using a chiral SU(3) model and their results indicate that the density dependence of the isospin asymmetry is appreciable for the kaon and antikaon optical potentials. On the other hand, subthreshold kaon production in heavy-ion collisions depends on some detailed implementations of the transport model [212, 213]. Therefore, extracting useful information on the high density behavior of the nuclear symmetry energy from subthreshold kaon production in heavy-ion collisions induced by neutron-rich nuclei needs further studies from both experimental and theoretical sides.

Besides the K^0/K^+ ratio, the Σ^-/Σ^+ ratio has also been proposed as a probe of the high density behavior of the nuclear symmetry energy based on the UrQMD model (version 1.3) calculations [105]. Shown in Fig.34 is the time evolution of the π^-/π^+ ratios (left-hand side) and the Σ^-/Σ^+ ratios (right-hand side) calculated with a stiff symmetry energy $F_1^{\gamma=1}$ and a soft symmetry energy $F_2^{a=3}$ for the reaction ^{132}Sn+^{132}Sn at $E_{\rm beam} = 1.5A$, $2.5A$, $3.5A$ GeV and $b = 2$ fm, and ^{112}Sn+^{112}Sn at $E_b = 3.5A$ GeV and $b = 2$ fm. It is seen that the Σ^-/Σ^+ ratio is sensitive to the density dependence of the symmetry energy for neutron-rich ^{132}Sn+^{132}Sn collisions, but insensitive to that for the nearly symmetric ^{112}Sn+^{112}Sn collisions. For ^{132}Sn+^{132}Sn at $E_b = 1.5A$ GeV, the Σ^-/Σ^+ ratio calculated with the stiff symmetry energy ($F_1^{\gamma=1}$) is higher than the one with the soft symmetry energy ($F_2^{a=3}$). As the beam energy increases, the Σ^-/Σ^+ ratio falls and the difference between the Σ^-/Σ^+ ratios calculated with $F_1^{\gamma=1}$ and $F_2^{a=3}$ reduces strongly. As the beam energy increases further, at $E_b = 3.5A$ GeV the Σ^-/Σ^+ ratio falls further but the difference between the Σ^-/Σ^+ ratios calculated with $F_1^{\gamma=1}$ and $F_2^{a=3}$ appears again, the Σ^-/Σ^+ ratio with soft symmetry energy now becoming higher than that with the stiff one. For pions, the results indicate that the ratio π^-/π^+ at high energies (as in the case with $E_b = 3.5A$ GeV) becomes insensitive to the symmetry energy. The difference between the Σ^-/Σ^+ ratio and the π^-/π^+ ratio can be understood from the fact that, like nucleons, $\Sigma^\pm$ hyperons are under the influence of the mean field produced by the sur-

rounding nucleons, as soon as they are produced. The symmetry potential of hyperons thus play an important dynamic role and results in a strong effect on the ratio of the negatively to positively charged Σ hyperons.

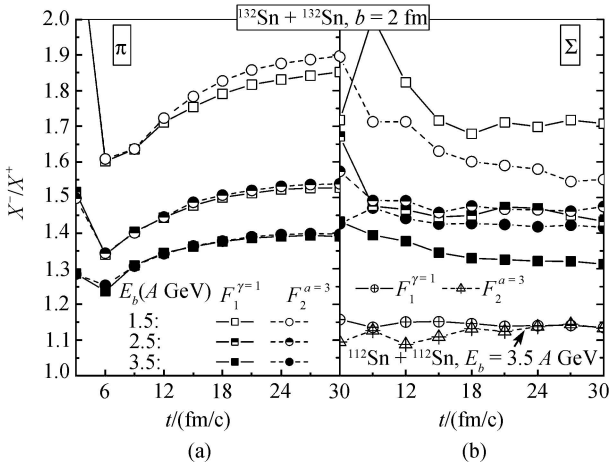

Fig.34 The ratios π^-/π^+ **(a)** and Σ^-/Σ^+ **(b)** for the collisions ^{132}Sn $+^{132}$ Sn ($E_b = 1.5A$, $2.5A$, and $3.5A$ GeV; $b = 2$ fm) and ^{112}Sn $+^{112}$ Sn ($E_b = 3.5A$ GeV; $b = 2$ fm), calculated with the different symmetry potentials $F_1^{\gamma=1}$ and $F_2^{a=3}$. Taken from Ref. [105].

7 Summary and outlook

Heavy-ion collisions induced by neutron-rich nuclei provides a unique opportunity for investigating the properties of the isospin asymmetric nuclear matter, especially the density dependence of the nuclear symmetry energy. To extract useful information from these collisions, transport models have been found to be extremely useful. Applications of these models have helped us understand not only the isospin dependence of the in-medium nuclear effective interactions but also that of the thermal, mechanical and transport properties of asymmetric nuclear matter. These information, particularly the density dependence of the nuclear symmetry energy, are very important for both nuclear physics and astrophysics. Significant progress has been made in recent years in determining the density dependence of the nuclear symmetry energy. Based on transport model calculations, a number of sensitive probes of the symmetry energy have been identified. In particular, the momentum dependence in both the isoscalar and isovector parts of the nuclear potential was found to play an important role in extracting accurately the density dependence of the symmetry energy. From comparison of results from the transport model with recent experimental data on isospin diffusion from NSCL/MSU, a symmetry energy of $E_{\rm sym}(\rho) \approx 31.6(\rho/\rho_0)^\gamma$ with $\gamma = 0.69 - 1.05$ at subnormal densities, which corresponds to the isospin and momentum dependent MDI interaction with $x = 0$ and -1, has been extracted. This conclusion is consistent with those extracted from studying other observables such as the isoscaling data and the neutron-skin thickness in ^{208}Pb.

Although considerable progress has been made in determining the density dependence of the nuclear symmetry energy at sub-normal densities, probing the high-density behavior of the nuclear symmetry energy remains a major challenge. Our current knowledge on the density dependence of the nuclear symmetry energy can be seen from Fig. 35, where predictions from several typical theoretical models [10, 18, 216] are compared with the phenomenological constraints that have been obtained from model analysis of experimental data. The constraints labeled $x = 0$ and $x = -1$ were extracted from studying the isospin diffusion in the reaction of ^{124}Sn +^{112}Sn at $E_{\rm beam} = 50$ AMeV within an isospin and momentum dependent transport model [99, 116−118]. For this particular reaction, the maximum density reached is about $1.2\rho_0$. Moreover, it was shown that the neutron-skin thickness in ^{208}Pb calculated within the Hartree-Fock approach using the same underlying Skyrme interactions as the ones labeled $x = 0$ and $x = -1$ is consistent with the available experimental data [119−121]. The symmetry energy labeled as FSU-Gold was calculated within an RMF model using an accurately calibrated parameter set such that it reproduces both the giant monopole resonance in ^{90}Zr and ^{208}Pb as well as the isovector giant dipole resonance of ^{208}Pb [122]. We note

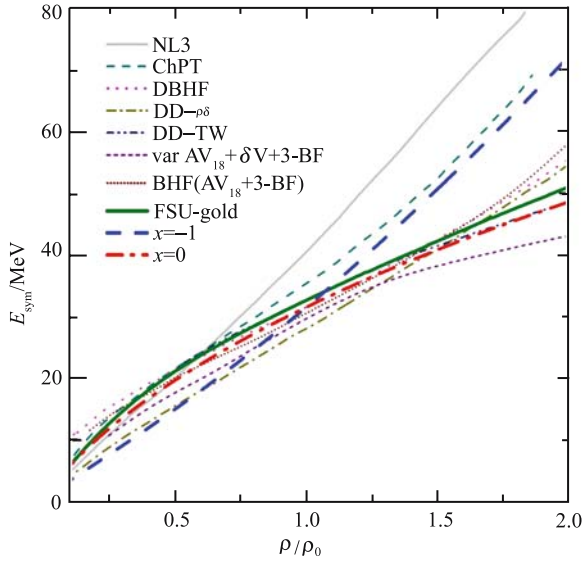

Fig.35 (*Color online*) Density dependence of the nuclear symmetry energy using the MDI interaction with $x = 0$ and $x = -1$ and other many-body theories predictions (data are taken from Refs. [18, 122, 216]). Taken from Ref. [113].

that the constraint obtained from the isoscaling analysis is also consistent with the FSU-gold and the $x = 0$ case [123]. At present, these results represent the best phenomenological constraints on the nuclear symmetry energy at sub-normal densities.

Although all predicted nuclear symmetry energies shown in Fig. 35 are close to the existing constraints at low densities, they diverge widely at supra-normal densities, including those from the MDI interaction with $x = -1$ and that with $x = 0$ as well as the FSU-Gold. Since there are currently no experimental constraints on the high density behavior of the nuclear symmetry energy, more work is thus needed. In particular, experimental data including neutrons from reactions with neutron-rich beams in a broad energy range will be useful for studying the behavior of the symmetry energy at high densities. We have reviewed recent theoretical progress in identifying the observables in heavy-ion collisions induced by high energy radioactive nuclei that are sensitive to the high density behavior of the nuclear symmetry energy. A plethora of potentially sensitive probes have been found, and they include the π^-/π^+ ratio, isospin fractionation, n-p differential flow, double $\mathrm{n/p}$ and π^-/π^+ ratio, double n-p differential transverse flow as well as the K^0/K^+ and Σ^-/Σ^+ ratios. Studying these observables in future experiments at high energy radioactive beam facilities is expected to lead to significant constraints on the behavior of the symmetry energy at supra-normal densities. Since transport models are essential in extracting these constraints from the experimental data, the continuous development of a practically implementable quantum transport theory for nuclear reactions induced by radioactive beams is important but poses a great challenge.

Acknowledgements This work was supported in part by the National Natural Science Foundation of China under Grant Nos. 10575071 and 10675082, MOE of China under project NCET-05-0392, Shanghai Rising-Star Program under Grant No. 06QA14024, the SRF for ROCS, SEM of China, the US National Science Foundation under Grant Nos. PHY-0652548 and PHY-0456890, PHY-0457265, the Welch Foundation under Grant No. A-1358, and the Research Corporation.

References

1. Li B. A., Ko C. M., and Bauer W., topical review, Int. Jour. Mod. Phys. E,1998, 7: 147
2. Isospin Physics in Heavy-Ion Collisions at Intermediate Energies, Eds. Li Bao-An and Udo Schröder W., Nova Science Publishers, Inc, New York, 2001
3. Danielewicz P., Lacey R., and Lynch W. G., Science, 2002, 298: 1592
4. Lattimer J. M. and Prakash M., Science, 2004, 304: 536
5. Baran V., Colonna M., Greco V., and Di Toro M., Phys. Rep., 2005, 410: 335
6. Steiner A. W., Prakash M., Lattimer J. M., and Ellis P. J., Phys. Rep., 2005, 411: 325
7. Myers W. D. and Swiatecki W. J., Nucl. Phys. A, 1996, 81: 1
8. Pomorski K. and Dudek J., Phys. Rev. C, 2003, 67: 044316
9. Bombaci I., in: Isospin Physics in Heavy-Ion Collisions at Intermediate Energies, Eds. Li Bao-An and Udo Schröder W., Nova Science Publishers, Inc, New York, 2001: 35
10. Dieperink A. E. L., Dewulf Y., Van Neck D., Waroquier M., and Rodin V., Phys. Rev. C, 2003, 68: 064307
11. Shlomo S. and Youngblood D. H., Phys. Rev. C,1993, 47: 529
12. Youngblood D. H. et al., Phys. Rev. Lett., 1999, 82: 691
13. Brueckner K. A., Coon S. A. and Dabrowski J., Phys. Rev., 1967, 168: 1184
14. Siemens P. J., Nucl. Phys., 1970, A141: 225
15. Sjöberg O., Nucl. Phys., 1974, A222: 161
16. Cugnon J., Deneye P., and Lejeune A., Z. Phys. A, 1987, 328: 409
17. Bombaci I. and Lombardo U., Phys. Rev. C, 1991, 44: 1892
18. Zuo W., Lejeune A., Lombardo U., and Mathiot J. F., Eur. Phys., 2002, J. A 14: 469
19. Müther H., Prakash M., and Ainsworth T. L., Phys. Lett., 1987, B199: 469
20. ter Haar B. and Malfliet R., Phys. Rep., 1987, 149: 207
21. Sumiyoshi K., Toki H., and Brockmann R., Phys. Lett., 1992, B276: 393
22. Huber H., Weber F., and Weigel M. K., Phys. Lett., 1993, B317: 485
23. Huber H., Weber F., and Weigel M. K., Phys. Rev. C, 1994, 50: R1287
24. van Dalen E. N. E., Fuchs C., and Faessler A., Nucl. Phys. 2004, A741: 227
25. van Dalen E. N. E., Fuchs C., and Faessler A., Phys. Rev. Lett., 2005, 95: 022302
26. Ma Z. Y., Rong J., Chen B. Q., Zhu Z. Y., and Song H. Q., Phys. Lett. B, 2004, 604: 170
27. Sammarruca F., Barredo W., and Krastev P., Phys. Rev. C, 2005, 71: 064306
28. Müther H. and Polls A., Prog. Part. Nucl. Phys., 2000, 45: 243
29. Dewulf Y., Van Neck D., and Waroquier M., Phys. Rev. C, 2002, 65: 054316
30. Carlson J., Morales J., Jr., Pandharipande V. R., and Ravenhall D. G., Phys. Rev. C, 2003, 68: 025802
31. Dickhoff W. H. and Barbieri C., Prog. Part. Nucl. Phys., 2004, 52: 377
32. Friedman B. and Pandharipande V. R., Nucl. Phys., 1981, A361: 502
33. Lagaris I. E. and Pandharipande V. R., Nucl. Phys., 1981, A369: 470
34. Wiringa R. B., Fiks V., and Fabrocini A., Phys. Rev. C, 1988, 38: 1010
35. Akmal A., Pandharipande V. R., and Ravenhall D. G., Phys. Rev. C, 1998, 58: 1804
36. Mukherjee A. and Pandharipande V. R., Phys. Rev. C, 2007, 75: 035802
37. Serot B. D. and Walecka J. D., Int. Jour. Mod. Phys. E, 1997, 6: 515
38. Furnstahl R. J., Lect. Notes Phys., 2004, 641: 1

39. Prakash M. and Ainsworth T. L., Phys. Rev. C, 1987, 36: 346
40. Lutz M., Friman B., and Ch. Appel, Phys. Lett., 2000, B474: 7
41. Finelli P., Kaiser N., Vretenar D., and Weise W., Nucl. Phys., 2004, A435: 449
42. Vretenar D. and Weise W., Lect. Notes Phys., 2004, 641: 65
43. Fritsch S., Kaiser N., and Weise W., Nucl. Phys., 2005, A750: 259
44. Finelli P., Kaiser N., Vretenar D., and Weise W., Nucl. Phys., 2006, A770: 1
45. Serot B. D. and Walecka J. D., Adv. Nucl. Phys., 1986, 16: 1
46. Chin S. A., Ann. Phys. (N. Y.), 1977, 108: 301
47. Horowitz C. J. and Serot B. D., Nucl. Phys., 1987, A464: 613
48. Serot B. D. and Uechi H., Ann. Phys. (N. Y.), 1987, 179: 272
49. Glendenning N. K., Phys. Lett., 1982, B114: 392
50. Hirata D., et al., Phys. Rev. C, 1991, 44: 1467
51. Sugahara Y. and Toki H., Nucl. Phys., 1994, A579: 557
52. Reinhard P. -G., Rep. Prog. Phys., 1989, 52: 439
53. Ring P., Prog. Part. Nucl. Phys., 1996, 37: 193
54. Miller L. D., Phys. Rev. C, 1974, 9: 537
55. Brockmann R., Phys. Rev. C, 1978, 18: 1510
56. Jaminon M., Mahaux C., and Rochus P., Nucl. Phys., 1981, A365: 371
57. Horowitz C. J. and Serot B. D., Nucl. Phys., 1983, A399: 529
58. Bouyssy A., Mathiot J. -F., Van Giai N., and Marcos S., Phys. Rev. C, 1987, 36: 380
59. Lopez-Quelle M., et al., Nucl. Phys. A, 1988, 483: 479
60. Bernardos P., Fomenko V. N., Nguyen Van Giai, Quelle M. L., Marcos S., Niembro R., and Savushkin L. N., Phys. Rev. C, 1993, 48: 2665
61. Werner T. R., et al., Phys. Lett., 1994, B333: 303
62. Dao T. Khoa, Von Oertzen W., and Ogloblin A. A., Nucl. Phys., 1996, A602: 98
63. Vautherin D. and Brink D. M., Phys. Rev. C, 1972, 5: 626
64. Brack M., Guet C., and Hakansson H. -B., Phys. Rep., 1985, 123: 275
65. Stone J. R. and Reinhard P. -G., Prog. Part. Nucl. Phys., 2007, 58: 587
66. Kolehmainen K., et al., Nucl. Phys., 1985, A439: 535
67. Treiner J., et al., Ann. Phys. (N.Y.), 1986, 170: 406
68. Bandyopadhyay D., Samanta C., Samaddar S. K., and De J. N., Nucl. Phys., 1990, A511: 1
69. Li Z. H., Lombardo U., Schulze H. -J., Zuo W., Chen L. W., and Ma H. R., Phys. Rev. C, 2006, 74: 047304
70. Li B. A. and Yennello S. J., Phys. Rev. C, 1995, 52: 1746(R)
71. Li B. A., Ren Z. Z., Ko C. M., and Yennello S. J., Phys. Rev. Lett., 1996, 76: 4492
72. Li B. A., Ko C. M., and Ren Z. Z., Phys. Rev. Lett., 1997, 78: 1644
73. Li B. A. and Ko C. M., Nucl. Phys., 1997, A618: 498
74. Chen L. W., Ge L. X., Zhang X. D., and Zhang F. S., J. Phys. G, 1997, 23: 211
75. Chen L. W., Zhang F. S. and Jin G. M., Phys. Rev. C, 1998, 58: 2283
76. Baran V., Colonna M., Di Toro M., and Larionov A. B., Nucl. Phys., 1998, A632: 287
77. Chen L. W., Zhang F. S., Jin G. M., and Zhu Z. Y., Phys. Lett., 1999, B459: 21
78. Zhang F. S., Chen L. W., Ming Z. Y., and Zhu Z. Y., Phys. Rev. C, 1999, 60: 064604
79. Xu H. S., et al., Phys. Rev. Lett., 2000, 85: 716
80. Chen L. W., Zhang F. S., and Zhu Z. Y., Phys. Rev. C, 2000, 61: 067601
81. Zhang F. S., Chen L. W., Li W. F., and Zhu Z. Y., Eur. Phys. J., 2000, A9: 149
82. Tan W. P., et al., Phys. Rev. C, 2001, 64: 051901(R)
83. Baran V., Colonna M., Di Toro M., Greco V., and Zielinska-Pfabé M., and Wolter H. H., Nucl. Phys., 2002, A703: 603
84. Tsang M. B., et al., Phys. Rev. Lett., 2001, 86: 5023
85. Li B. A., Sustich A. T., and Zhang B., Phys. Rev. C, 2001, 64: 054604
86. Li B. A., Phys. Rev. Lett., 2000, 85: 4221
87. Special issue on Radioactive Nuclear Beams, Edited by I. Tanihata [Nucl. Phys., 2001, A693]
88. Li B. A., Phys. Rev. Lett., 2002, 88: 192701
89. Li B. A., Nucl. Phys., 2002, A708: 365
90. Chen L. W., Greco V., Ko C. M., and Li B. A., Phys. Rev. Lett., 2003, 90: 162701
91. Chen L. W., Ko C. M., and Li B. A., Phys. Rev. C, 2003, 68: 014605
92. Chen L. W., Ko C. M., and Li B. A., Phys. Rev. C, 2003, 68: 017601
93. Chen L. W., Ko C. M., and Li B. A., Nucl. Phys., 2003, A729: 809
94. A. Ono, P. Danielewicz, Friedman W. A., Lynch W. G., and Tsang M. B., Phys. Rev. C, 2003, 68: 051601 (R)
95. Liu J. Y., Guo W. J., Xing Y. Z., and Liu H., Nucl. Phys., 2003, A726: 123
96. Chen L. W., Ko C. M., and Li B. A., Phys. Rev. C, 2004, 69: 054606
97. Li B. A., Das C. B., Das Gupta S., and Gale C., Phys. Rev. C, 2004, 69: 011603 (R)
98. Li B. A., Nucl. Phys., 2004, A735: 563
99. Shi L. and Danielewicz P., Phys. Rev. C, 2003, 68: 064604
100. Li B. A., Phys. Rev. C, 2004, 69: 034614
101. Rizzo J., Colonna M., Di Toro M., and Greco V., Nucl. Phys., 2004, A732: 202
102. Li B. A., Yong G. C., and Zuo W., Phys. Rev. C, 2005, 71: 014608
103. Li B. A., Yong G. C., and Zuo W., Phys. Rev. C, 2005, 71: 044604
104. Zhang Y. and Li Z., Phys. Rev. C, 2005, 71: 024604
105. Li Q., Li Z., Zhao E., and Gupta R. K., Phys. Rev. C, 2005, 71: 054907
106. Tian W. D., et al., Chin. Phys. Lett., 2005, 22: 306
107. Muller H. and Serot B., Phys. Rev. C, 1995, 52: 2072
108. Gaitanos T., Di Toro M., Type S., Baran V., Fuchs C., Greco V., and Wolter H. H., Nucl. Phys., 2004, A732: 24
109. Li Q. F., Li Z. X., Soff S., Gupta R. K., Bleicher M. and Stöcker H., Phys. Rev. C, 2005, 72: 034613; ibid, nucl-th/0509070
110. Ferini G., Gaitanos T., Colonna M., Di Toro M., and Wolter H. H., Phys. Rev. Lett., 2004, 92: 062701
111. Ferini G., Colonna M., Gaitanos T., and Di Toro M., Nucl. Phys., 2005, A762: 147
112. Li Bao-An, Chen Lie-Wen, Champak B. Das, Subal Das Gupta, Charles Gale, Ko Che Ming , Yong Gao-Chan, and Zuo Wei, Proc. AIP, 2005, 791: 22; arXiv:nucl-th/0504069
113. Yong G. C., Li B. A., and Chen L. W., arXiv:nucl-th/0703042, Phys. Lett. B, 2007 (in press)
114. Bertsch G. F. and Das Gupta S., Phys. Rep., 1988, 160: 189

115. Aichelin J., Phys. Rep., 1991, 202: 233
116. Li B. A. and Chen L. W., Phys. Rev. C, 2005, 72: 064611
117. Tsang M. B., et al., Phys. Rev. Lett., 2004, 92: 062701
118. Chen L. W., Ko C. M., and Li B. A., Phys. Rev. Lett., 2005, 94: 032701
119. Steiner A. W. and Li B. A., Phys. Rev. C, 2005, 72: 041601 (R)
120. Li B. A. and Andrew W. Steiner, Phys. Lett. B, 2006, 642: 436
121. Chen L. W., Ko C. M. and Li B. A., Phys. Rev. C, 2005, 72: 064309
122. Todd-Rutel B. G. and Piekarewicz J.,, Phys. Rev. Lett., 2005, 95: 122501
123. Shetty D., Yennello S. J., and Souliotis G. A., Phys. Rev. C, 2007, 75: 034602
124. Prakash M. and Bedell K. S., Phys. Rev. C, 1985, 32: 1118
125. Baron E., Cooperstein J., and Kahana S., Phys. Rev. Lett., 1985, 55: 126; Nucl. Phys., 1985, A440: 744
126. Kahana S. H., Ann. Rev. Nucl. Part. Sci., 1989, 39: 231
127. Lattimer J. M., Pethick C. J., Prakash M., and Haensel P., Phys. Rev. Lett., 1991, 66: 2701
128. Sumiyoshi K. and Toki H., Astro. Phys. Journal, 1994, 422: 700
129. Lee C. -H., Phys. Rep., 1996, 275: 255
130. Das C. B., Das Gupta S., Gale C., and Li B. A., Phys. Rev. C, 2003, 67: 034611
131. Wiringa R. B., Phys. Rev. C, 1988, 38: 2967
132. Zuo W., Gao L. G., Li B. A., Lombardo U., and Shen C. W., Phys. Rev. C, 2005, 72: 014005
133. Satchler G. R., Chapter 9: Isospin Dependence of Optical Model Potentials, in: Isospin in Nuclear Physics, Wilkinson D. H. (Ed.), North-Holland, Amsterdam, 1969: 391−456
134. Hoffmann G. W. and Coker W. R., Phys. Rev. Lett., 1972, 29: 227
135. Hodgson P. E., The Nucleon Optical Model, World Scientific, Singapore, 1994: 613−651
136. Koning A. J. and Delarocje J. P., Nucl. Phys., 2003, A713: 231
137. Jaminon M. and Mahaux C., Phys. Rev. C, 1989, 40: 354
138. Negele J. W. and Orland H., Quantum Many-Particle System, Perseus Books Publishing, L. L. C., 1998
139. Li B. A., Phys. Rev. C, 2004, 69: 064602
140. Behera B., Routray T. R., Pradhan A., Patra S. K., and Sahu P. K., Nucl., Phys. A, 2005, 753: 367
141. Sjöberg O., Nucl. Phys., 1976, A265: 511
142. Bertsch G. F., Kruse H., and Das Gupta S., Phys. Rev. C, 1984, 29: 673
143. Negele J. W. and Yazaki K., Phys. Rev. Lett., 1981, 62: 71
144. Pandharipande V. R. and Pieper S. C., Phys. Rev. C, 1991, 45: 791
145. Li G. Q. and Machleidt R., Phys. Rev. C, 1993, 48: 1702; ibid, C, 1994, 49: 566
146. Schulze H. -J., et al., Phys. Rev. C, 1997, 55: 3006; A. Schnell et al., ibid, C, 1998, 57: 806
147. Persram D. and Gale C., Phys. Rev. C, 2002, 65: 064611
148. Giansiracusa G., Lombardo U., and Sandulescu N., Phys. Rev. C, 1996, 53: R1478
149. Kohno M., Higashi M., Watanabe Y., and Kawai M., Phys. Rev. C, 1998, 57: 3495
150. Li Qingfeng, Li Zhuxia, and Mao Guangjun, Phys. Rev. C, 2000, 62: 014606
151. Chen L. W., et al., Phys. Rev. C, 2001, 64: 064315
152. Danielewicz P., Acta. Phys. Polon., 2002, B33: 45, and references therein
153. Sammrruca F. and Krastev P., nucl-th/0506081
154. Bertsch G. F., Brown G. E., Koch V., and Li B. A., Nucl. phys., 1988, A490: 745
155. Mao G. J., Li Z. X., Zhuo Y. Z., Han Y. L., and Yu Z. Q., Phys. Rev. C, 1994, 49: 3137; Mao G. G., Li Z. X., and Zhuo Y. Z., ibid, C, 1996, 53: 2933
156. Mao G. J., Li Z. X., Zhuo Y. Z., and Zhao E. G., Phys. Rev. C, 1997, 55: 792
157. Gaitanos T., Fuchs C., and Wolter H. H., Phys. Lett, 2005, B609: 241
158. Prakash M., Kuo T. T. S., and Das Gupta S., Phys. Rev. C, 1988, 37: 2253
159. Farine M., et al., Z. Phys., 1991, A339: 363
160. Gale C., Bertsch G., and Das Gupta S., Phys. Rev. C, 1987, 35: 1666
161. Welke G. M., et al., Phys. Rev. C, 1988, 38: 2101
162. Gale C., et al., Phys. Rev. C, 1990, 41: 1545
163. Pan Q. and Danielewicz P., Phys. Rev. Lett., 1993, 70: 2062
164. Zhang J., et al., Phys. Rev. C, 1994, 50: 1617
165. Greco V., et al., Phys. Rev. C, 1999, 59: 810
166. Danielewicz P., Nucl. Phys., 2000, A673: 375
167. Rami F., et al., Phys. Rev. Lett., 2000, 84: 1120
168. Fujiwara M., private communications, 2005
169. Piekarewicz J., private communications, 2005
170. Colo G., private communications, 2005
171. Li B. A., Danielewicz P., and Lynch W. G., Phys. Rev. C, 2005, 71: 054603
172. Brown B. A., Phys. Rev. Lett., 2000, 85: 5296
173. Horowitz C. J. and Piekarewicz J., Phys. Rev. Lett., 2001, 86: 5647
174. Horowitz C. J., and Piekarewicz J., Phys. Rev. C, 2002, 66: 055803
175. Typel S. and Brown B. A., Phys. Rev. C, 2001, 64: 027302
176. Furnstahl R. J., Nucl. Phys. A, 2002, 706: 85
177. Karataglidis S., Amos K., Brown B. A., and Deb P. K., Phys. Rev. C, 2002, 65: 044306
178. Friedrich J. and Reinhard P. -G., Phys. Rev. C, 1986, 33: 335
179. Brown B. A., Phys. Rev. C, 1998, 58: 220
180. Chen L. W. and Zhang F. S., High Energy Phys. and Nucl. Phys., 1999, 23: 1197 (in Chinese)
181. Stone J. R., Miller J. C., Koncewicz R., Stevenson P. D., and Strayer M. R., Phys. Rev. C, 2003, 68: 034324
182. Starodubsky V. E. and Hintz N. M., Phys. Rev. C, 1994, 49: 2118
183. Clark B. C., Kerr L. J., and Hama S., Phys. Rev. C, 2003, 67: 054605
184. Krasznahorkay A., et al., Nucl. Phys. A, 2004, 731: 224
185. Horowitz C. J., and Piekarewicz J., Phys Rev. C, 2001, 63: 025501
186. Jefferson Laboratory Experiment E-00-003, spokesperson Michaels R., Souder P. A., and Urciuoli G. M.
187. Yako K., Sagawa H., and Sakai H., Phys Rev. C, 2006, 74: 051303(R)
188. Li B. A., Phys. Rev. C, 2003, 67: 017601
189. Bertsch G. F., Nature, 1980, 283: 280
190. Bonasera A. and Bertsch G. F., Phys. Let. B, 1987, 195: 521
191. Lynch W. G., Sobotka L. G. and Tsang M. B., private communications, 2006
192. Famiano M. A., et al., Phys. Rev. Lett., 2006, 97: 052701

193. Li B. A., Chen L. W., Yong G. C., and Zuo W., Phys. Lett. B, 2006, 634: 378
194. Yong G. C., Li B. A., Chen L. W., and Zuo W., Phys. Rev. C, 2006, 73: 034603
195. Stock R., Phys. Rep., 1986, 135: 259
196. Li B. A. and Bauer W., Phys. Rev. C, 1991, 44: 450
197. Yong G. C., Li B. A., Chen L. W., Phys. Rev. C, 2006, 74: 064617
198. Stöcker H. and Greiner W., Phys. Rep.,1986, 137: 277
199. Cassing W., Metag V., Mosel U., and Niita K., Phys. Rep., 1990, 188: 363
200. Reisdorf W. and Ritter H. G., Annu. Rev. Nucl. Part. Sci., 1997, 47: 663
201. Htun M. M., et al., Phys. Rev. C, 1999, 59: 336, and references therein
202. Venema L., et al., Phys. Rev. Lett., 1993, 71: 835
203. Leifels Y., et al., Phys. Rev. Lett., 1993, 71: 963
204. Lambrecht D., et al., Z. Phys., 1994, A350: 115
205. Bass S. A., Hartnack C., Stöcker H., and Greiner W., Z. Phys., 1995, A352: 171
206. Larionov A. B., Cassing W., Greiner C., and Mosel U., Phys. Rev. C, 2000, 62: 064611
207. Bickley A., Famiano M. A., Lynch W. G., Westfall G. D., et al., private communications and their talks at the 2007 Town Meeting for the NSAC Long Range Plan, Chicago, January 19−21, 2007
208. Aichelin J. and Ko C. M., Phys. Rev. Lett., 1985, 55: 2661
209. Ko C. M. and Li G. Q., J. Phys. G, 1996, 22: 1673
210. Ko C. M., Koch V., and Li G. Q., Ann. Rev. Nucl. Part. Sci., 1997, 47: 505
211. Cassing W. and Bratkovskaya E. L., Phys. Rep., 1999, 308: 65
212. Kolomeitsev E. E., Hartnack C., Barz H. W., Bleicher M., Bratkovskaya E., Cassing W., Chen L. W., Danielewicz P., Fuchs C., Gaitanos T., Ko C. M., Larionov A., Reiter M., Gy. Wolf, and J. Aichelin, J. Phys. G, 2005, 31: S741
213. Fuchs C., Prog. Part. Nucl. Phys., 2006, 56: 1
214. Li Q., Li Z. X., Soff S., Raj K. Gupta, Bleicher M., and Stoecker H., J. Phys. G, 2005, 31: 1359
215. Lopez X., Kim Y. J., Herrmann N., et al. (FOPI Collaboration), Phys. Rev. C, 2007, 75: 011901(R)
216. Fuchs C., and Wolter H. H., Eur. Phys. J. A, 2006, 30: 5